AD-781 820

THE PHYSICS OF INTERFACE INTERACTIONS RELATED TO RELIABILITY OF FUTURE ELECTRONIC DEVICES

Thomas R. DiStefano, et al

IBM Thomas J. Watson Research Center

Prepared for:

Air Force Cambridge Research Laboratories
Advanced Research Projects Agency

31 July 1973

DISTRIBUTED BY:

NTIS
National Technical Information Service
U. S. DEPARTMENT OF COMMERCE
5285 Port Royal Road, Springfield Va. 22151

REPORT DOCUMENTATION PAGE

READ INSTRUCTIONS BEFORE COMPLETING FORM

1. REPORT NUMBER
AFCRL-TR-74-0194

2. GOVT ACCESSION NO.

3. RECIPIENT'S CATALOG NUMBER

4. TITLE (and Subtitle)
THE PHYSICS OF INTERFACE INTERACTIONS RELATED TO RELIABILITY OF FUTURE ELECTRONIC DEVICES

5. TYPE OF REPORT & PERIOD COVERED
Semi-Annual Technical Report No. 2

6. PERFORMING ORG. REPORT NUMBER

7. AUTHOR(s)
Thomas H. DiStefano
King-Ning Tu

8. CONTRACT OR GRANT NUMBER(s)
F19628-73-C-0006

9. PERFORMING ORGANIZATION NAME AND ADDRESS
IBM Thomas J. Watson Research Center
International Business Machines Corporation
P. O. Box 218, Yorktown Heights, New York 10598

10. PROGRAM ELEMENT, PROJECT, TASK AREA & WORK UNIT NUMBERS
61101D, 2180
Task & Work Unit n/a

11. CONTROLLING OFFICE NAME AND ADDRESS
Air Force Cambridge Research Laboratories (LQ)
L. G. Hanscom Field
Bedford, Massachusetts 01730

12. REPORT DATE
31 July 1973

13. NUMBER OF PAGES
97

14. MONITORING AGENCY NAME & ADDRESS(If different from Controlling Office)

15. SECURITY CLASS. (of this report)
Unclassified

15a. DECLASSIFICATION/DOWNGRADING SCHEDULE

16. DISTRIBUTION STATEMENT (of this Report)

A - Approved for public release; distribution unlimited.

17. DISTRIBUTION STATEMENT (of the abstract entered in Block 20, if different from Report)

18. SUPPLEMENTARY NOTES

This research was supported by the Defense Advanced Research Projects Agency.

19. KEY WORDS (Continue on reverse side if necessary and identify by block number)

Glass-metal reaction	Phosphorous segregation in SiO_2
Metal-silicon reaction	Si-SiO_2 interface polarization
Metal-silicide formation	EPR studies in SiO_2
Dielectric breakdown of SiO_2	Reflectivity studies in SiO_2
Valence band width in SiO_2	Switching in $Ge_{15}Te_{85}$

20. ABSTRACT (Continue on reverse side if necessary and identify by block number)

A theoretical model was developed to describe the problem of dielectric breakdown in wide gap insulators which have a low hole mobility. Electrons injected by Fowler-Nordheim tunneling are accelerated in the electric field and leave behind a residue of positive charge which enhances the cathode field and leads to a regenerative enhancement of the ionization. The calculation for the particular case of SiO_2 shows a negative resistance type of instability and a breakdown field which increases at small

DD FORM 1 JAN 73 1473 EDITION OF 1 NOV 65 IS OBSOLETE electrode separation.

In order to understand hole transport and mobility in SiO_2, we have studied optical transitions by using uv reflectivity to investigate structures near the band edge as a function of the Si-O-Si bond angle. Structure is seen in the optical data of cristoballite which indicates that the uppermost narrow valence band has a finite bandwidth due to wavefunction overlap.

Phosphorus precipitates were found on the interface between P-doped silicon and thermally grown SiO_2. The technique of scanning internal photoemission was used to form an image of the phosphorus islands whose size and spacing depend upon the areal density of phosphorus in the oxidized silicon. The islands were found to completely cover the silicon surface for an areal density of $5 \times 10^{14}/cm^2$.

Resistive switching was studied in $Ge_{15}Te_{85}$ by transmission electron-microscopy. Three resistive states were observed, consisting of a wholly amorphous structure, Te crystallites in an amorphous GeTe matrix, and Te crystallites in a crystalline GeTe matrix. Switching was observed between the latter two but structural degradation resulted.

In the area involving the structural instability of glass-metal interfaces, we have performed a systematic study of interfacial reactions between thermally-grown SiO_2 and three transition metals; V, Ti, and Nb. We found that there interfaces became unstable at temperatures above 700°C and destruction of the structure of SiO_2 followed. This is significant because active transition metals are often used to increase the adhesion of a second metal to the surface of SiO_2.

TABLE OF CONTENTS

THE PHYSICS OF INTERFACE INTERACTIONS RELATED TO RELIABILITY OF FUTURE ELECTRONIC DEVICES

INTRODUCTION

The overall purpose of our work continues to be the investigation of fundamental phenomena that directly impact the performance of projected electronic device configurations. We have been probing and reporting on various possible approaches to understanding the many phenomena which can influence the reliability of integrated devices including such areas as polarization effects on interface contact barriers and carrier injection into SiO_2; dielectric breakdown mechanisms and models, band structure in insulation; radiation-induced charge in insulators; trapping states in insulation interfaces such as MNOS structures; switching and conduction mechanisms in doped transition metal oxides; drift of charged carriers through SiO_2 and impurity induced crystallization; and reactions at metal-Si and metal-SiO_2 interfaces.

For the near future, we will concentrate on those programs which have proven to be of fundamental scientific importance and which underlie the significant degradation modes that can be foreseen. This provides the best chance for future extension of new device concepts. These include a more concerted effort theoretically to describe interface polarization effects and contact barrier drift, continued expansion of the theoretical dielectric breakdown model and its implications, description of radiation-induced charge carriers in SiO_2, and reaction kinetics at metal-SiO_2 (or Si) interfaces.

- We have developed an understanding of precisely what happens in the initial stages of dielectric breakdown in SiO_2. A simple model for dielectric breakdown was formulated on the basis of electron injection from blocking contacts and subsequent impact ionization of the lattice. Several predictions can be made, including the increased average breakdown field found for ultra-thin films of SiO_2. Ionizing radiation is predicted to reduce drastically the breakdown strength of SiO_2.

- The breakdown model predicts an increase in the breakdown field of greater than 100% for SiO_2 films 100 Å thick. For such thin films, the negative reistance portion of the curve disappears. This means that thin films about 100 Å thick, would have superior qualities as a gate insulator.

- For n-type silicon or for n-channel MOS devices, the phosphorus dopant from the silicon was found to precipitate onto any silicon surface which has been oxidized. This surface layer or phosphorus can cause a leakage channel to appear near the surfaces of heavily phosphorus doped silicon. As a result, the surface leakage path can destroy the operation of an ultra-small MOS transistor because the leakage path bridges the source and drain regions. It is expected that arsenic, the other n-type dopant, displays the same behavior.

- We have found that the optical properties of SiO_2 do not depend significantly upon the allotropic form of the material. The results indicate a valence band width of about 1 eV for the top valence band of SiO_2 crystoballite.

- We have found that certain metals can cause reliability problems when used as metallization on SiO_2 glass, especially where the combination is subjected to elevated temperatures. Metals that form both stable silicides and oxides, such as V, Ti, Cr, Nb, and Ta, may decompose SiO_2 thin films over a period of time, and thereby destroy the dielectric properties of the insulating film.

- In the area of Schottky barriers, we have finished a review of our current understanding of silicide formation and stability. We found that there is a distinct difference between the silicides formed by the metal-silicon reaction and by metal- glass reaction; the latter produce a metal-rich phase while the former produce a silicon-rich phase. This shows the signficance of having a thin oxide layer on the contact reaction between a Si wafer and a metallic films.

I. THE RELIABILITY OF SEMICONDUCTOR-INSULATOR INTERFACES

We have completed an investigation of a physical model of dielectric breakdown in SiO_2 thin films, including a study of the influence of the adjustable parameters and a study of several important predictions. This is the first quantitative model to describe exactly what occurs during the critical initial stages of dielectric breakdown in the dielectrics used in integrated circuits. The negative resistance type of breakdown is due to a distortion of the electric field caused by positive charge left in the insulator by the small amount of impact ionization produced by hot electrons. From this study, we find that the only parameter which has a significant effect on the calculated breakdown strength is the electron-phonon scattering length. A good fit to the experimental breakdown data for films below 1000 Å was obtained for a scattering length of 1.34 Å. The analysis was expanded to include relative effects of the mean free path λ_i for impact ionization of the valence band edge as well as the recombination cross section σ as calculated by several models. Neither were as important in determining breakdown as the electron-phonon scattering length.

The theory predicts the experimentally observed increase in breakdown strength for films thinner than ∿ 500 Å. The other important predictions need experimental verification: the threshold current for breakdown is found to increase dramatically with a decreasing film thickness, and the intrinsic breakdown voltage decreases in the presence of ionizing radiation.

By scanning internal photoemission measurements, we have seen evidence for the precipitation of phosphorus on Si-SiO_2 interfaces grown on phosphorus doped silicon. Apparently, the phosphorus that dissolves in the SiO_2 during oxidation of the doped silicon precipitates onto the interface during the period when the silicon is cooled from the oxidation temperature. Islands of phosphorus were seen as dark spots (low photoyield) on photoemission images of sodium stained Si-SiO_2 interfaces. These spots are absent from interfaces grown on lightly phosphorus doped silicon ($\sim 2 \times 10^{18}/cm^3$), while they completely cover an interface grown on a very heavily doped wafer ($\sim 5 \times 10^{20}/cm^3$). Samples in the intermediate range of doping show phosphorus rich islands on the Si-SiO_2 interface, with a diameter of up to 25 microns. The significant fact is that silicon surfaces are degraded by phosphorus which is introduced during the thermal oxidation of heavily doped silicon.

A. IMPACT IONIZATION MODEL FOR DIELECTRIC INSTABILITY AND BREAKDOWN

T. H. Di Stefano and M. Shatzkes

Dielectric breakdown in wide-bandgap insulators is an old problem which has long been considered in quite general terms from several points of view.[1,2] These treatments determine criteria for electronic instability and dielectric breakdown in terms of the behavior of a single electron in an infinite insulator which supports a uniform electric field. More recent theoretical work has resulted in a few microscopic models for dielectric breakdown in finite systems. The models fall into two classifications: an instability due to thermal runaway[3] in a system containing a relatively low energy excited electronic state; or an electronic avalanche[4,5] type of dielectric breakdown in which hot electrons impact bound electrons and ionize them from the valence band. By either a thermal or an avalanche model, the current-voltage relationship is found to have a negative resistance or dielectric instability due to a non-local regenerative mechanism. The avalanche model for electronic breakdown developed by O'dwyer[4] employs a distortion of the electric field in the insulator to obtain the non-local feedback necessary for the instability. In effect, the positive charge carriers produced during an avalanche drift to the cathode where they enhance the electric field which, in turn, leads to an increased electron injection current and a greater rate of impact ionization. The O'dwyer model is based on the assumption that the holes produced by impact ionization remain relatively mobile and that the electron energy distribution depends only upon the local electric field but not upon distance from the cathode. This set of assumptions is valid for many semiconductors, but it does not apply well to thin films of those wide-bandgap insulators with a very low hole mobility.

We present a simple theory for dielectric breakdown in materials such as SiO_2[6] for which the hole mobility is relatively small. The calculations are based on impact ionization of the insulator lattice by electrons injected from the cathode and subsequently heated by the electric field.[7] The theory is developed for the idealized case in which hole motion is negligible during the rapid breakdown process. It is assumed that during the short time required for breakdown, holes are cleared from the insulator largely by recombination and that drift in the electric field does not seriously influence the hole distribution or density in the insulator. As a specific example of this model, the breakdown voltage and the current-voltage relationship were calculated for the case of a thin layer of SiO_2. The breakdown voltage was found to depend significantly upon only one of the adjustable parameters, the one dimensional energy loss length. The recombination cross section and the ionization cross section have a rather small influence on the calculated breakdown voltage. The dependence of the average electric field at breakdown on thickness is calculated and found to increase rapidl below 200Å.

The principal features of the model are outlined in Fig. 1, which shows the valence and conduction bands in the insulator during the breakdown process. Since the bandgap[8] of SiO_2 is 9.0 eV, the threshold for impact ionization is 9 eV above the bottom of the conduction band, as marked by the dashed line in the figure. Electrons are injected into the insulator by Fowler-Nordheim tunneling from one of the electrodes. The tunneling current density J is of the form[9],

$$J = (q^3E^2/16\pi^2\hbar^2\Phi)e^{-[(32m^*)^{1/2}\ \Phi^{3/2}/3\hbar eE]} \qquad (1)$$

where Φ is the interface energy barrier, m* is the effective mass in the insulator, and E is the electric field at the cathode. For SiO_2, m*=.41 and Φ=4.2 eV. As will be shown, the results of the calculation of the field distortion in the insulator are independent of the level of injected current. Since the solution is insensitive to the level of injected current for high Φ contacts and low temperatures, we will use the approximate form for the Fowler-Nordheim current, and neglect temperature and image force lowering corrections.

The injected electrons are accelerated by the electric field so that after traversing a distance x, a high energy tail of the electron energy distribution has sufficient energy to ionize the lattice. Electrons above the ionization threshold are assumed to produce impact ionization with a mean length λ_i. Each impact ionization event leaves behind a low-mobility valence band hole. In this model, it is assumed that the hole moves an insignificant distance before it is anihilated by recombination with another injected electron. As a consequence of repeated impact ionization, a residual cloud of positive space charge is built up and the potential is distorted so as to enhance the cathode field. In turn, the enhanced field leads to impact ionization nearer the cathode, moving the sheet of positive charge closer to the cathode. The holes downstream from the major ionization region are removed by recombination. By a regeneration process, the positive charge sheet moves closer to the cathode, leading to an increase in the cathode field and a resulting increase in the injected electron current. At a critical point, an increase in current is accompanied by a decrease in total potential drop across the thin film. This point, at the beginning of the negative resistance regime, marks the onset of a dielectric breakdown instability.

In order to calculate the current-voltage relationship and to find the dielectric breakdown voltage of a thin dielectric, the rate of impact ionization is first determined. The problem is complicated by the fact that the electron energy distribution does not reach an equilibrium form in the sharply varying field of the insulator. It is both possible and necessary to determine the spacial evolution of the electron distribution, with the aid of a few simplifying approximations. The electron scattering events are assumed to be independent and to involve the loss of one LO phonon per collision which is assumed to be predominantly a forward scattering event. The electron energy distribution is obtained by considering the one dimensional projection of the scattering events to be a Poisson process. That is, the electron moves an average distance λ in the x direction between independent scattering events. The parameter λ is the <u>one dimensional</u> projection of the <u>phonon emission length</u>. This λ is not to be confused with the mean free path or momentum randomization length; indeed, the two can be quite different for the case of a predominantly forward scattering event. The probability that an electron will suffer n collisions in traversing a distance λ is,

$$P(n,x) = \frac{1}{n!}\left(\frac{x}{\lambda}\right)^n e^{-x/\lambda}. \qquad (2)$$

A discrete energy distribution curve at point x is obtained by allowing the electron to lose one phonon or $\hbar\omega$ in each collision. At x, the probability P is a function of the energy E,

$$P(x,E) = \frac{1}{(-E/\hbar\omega)!} \left(\frac{x}{\lambda}\right)^{-E/\hbar\omega} e^{-(x/\lambda)}, \qquad (3)$$

or, by the central limit theorem, the energy distribution is

$$D(x,E) \cong \frac{(1/\hbar\omega)}{\sqrt{2\pi(x/\lambda)}} e^{-\frac{(E/\hbar\omega + x/\lambda)^2}{2(x/\lambda)}} \qquad (4)$$

where E is the energy with respect to the initial energy.

For the case in which an electron ionizes the lattice as soon as it attains an energy of E_g above the conduction band edge, the rate of impact ionization or production of positive charge is then,

$$\dot{\rho}_+\Big|_i = J \frac{d}{dx} \int_{\phi(x)+E_g}^{0} D(x,E)\, dE. \qquad (5)$$

In the equilibrium condition, the rate of production of positive charge by ionization is equal to that of destruction by recombination.

$$\dot{\rho}_+\Big|_r = \frac{J\rho_+}{e} \int_{\phi(x)}^{0} \sigma(E)\, D(X,E)\, dE \qquad (6)$$

where $\sigma(E)$ is the energy dependent recombination cross section. The hole charge density ρ_+ is found to be independent of injected current J,

$$\rho_+ = \frac{e\frac{d}{dx} \int_{\phi(x)+E_g}^{0} D(x,E)\, dE}{\sigma(E_T) \int_{-\infty}^{\phi(x)} D(x,E)\, dE + \int_{\phi(x)}^{0} \sigma(E)\, D(x,E)\, dE}, \qquad (7)$$

where $\sigma(E)$ is the energy dependent recombination cross section and E_T is the limiting energy of electrons near the conduction band bottom. Here, the tail of the electron distribution which is calculated to be at or below the conduction band bottom is assumed to have a limiting energy[10] of $E_T=4\hbar\omega/3\pi$. Now the potential $\rho(x)$ can be found from a double integration of the net charge in the insulator.

$$\varphi(x) = \frac{1}{\varepsilon} \int dx \int dx \ (\rho_+ - \rho_-). \qquad (8)$$

In the usual situation, ρ_- is negligible in comparison to ρ_+. The potential V drop across a film of thickness d is found by the integration

the current corresponding to the V(d) is obtained from the Fowler-Nordheim equation(1) evaluated for the electric field at the cathode. From these two values for $\Delta x=d$, the J-V relationship is calculated for an insulator of thickness d.

Our impact ionization model is applied to the specific case of SiO_2, which may be somewhat less than ideal for two reasons. First, although the hole mobility in SiO_2 is quite small and unknown it must be finite. Since this mobility is undetermined at present, we leave it out of the calculation; however, more exact solution including the effect of hold motion are not expected to influence the general characteristics of the model. Another assumption which is not exact for SiO_2 is the phonon energy loss, which is taken to be the LO phonon energy $\hbar\omega=.153$ eV. At electron energies near the ionization threshold, phonons from other parts of the Brillouin zone contribute to the scattering but introduce an energy loss less than the full .153 eV. Since the relative cross sections are not known for scattering by the various types of phonons, we must retain the simple Einstein model for the phonon spectrum.

The results of the calculation are summarized in Figs. 2-4 for the application of the model to SiO_2. The J-V characteristic for a film of 1000 Å of SiO_2, in Fig. 2, displays an unstable negative resistance regime above a critical point on the knee of the curve at 95 Volts. Here, the family of curves corresponds to the J-V characteristic for three widely different values of λ_i the mean ionization path length. The recombination cross section $\sigma(E)$ is evaluated by using the Milne formula to estimate the cross section for radiative recombination. The third and most important parameter is λ, the one dimensional projection of the electron-phonon mean free path. The λ' was set to 1.34 Å to match the experimentally determined breakdown strength for films 1000 Å thick. Notice that the negative resistance instability occurs at very nearly the same foltage, independent of the mean ionization length λ_i for λ_i=0,10, and 100 Å. Apparently, the breakdown voltage is not influenced by the parameter λ_i. Below the critical point at the knee of the J-V curve, the current does not deviate appreciably from the Fowler-Nordheim value.

Insensitivity of the breakdown voltage to variations in the magnitude of the recombination cross-section is illustrated in Fig. 3. The curve labelled "Rose" in this figure is the result of the calculation using a recombination cross-section estimated according to qualitative arguments given by Rose.[11] This cross-section is

$$\sigma = \frac{\pi e^4}{\varepsilon^2} \frac{1}{E^2} .$$

Roughly this gives a cross-section which is larger than that of the

Milne-model by about a factor of 10^6. Yet the same breakdown voltage is obtained if a λ=1.68 Å is used in place of the λ=1.34 Å required in the Milne model.

In figure 4, the average field at breakdown, the breakdown voltage divided by the oxide film thickness, is plotted as a function of oxide thickness for the Milne recombination cross-section and λ=1.34 Å. There is little change in the average field for the thicker films, while for films thinner than ~ 200 Å there is a sharp increase in the average field.

In this calculations we have retained what we considered to be the essential characteristics of insulators such as SiO_2, i.e. the relative immobility of the hole, and a single active optical phonon. Neglect of hole motion and other energy loss mechanisms are approximations that reduced the complexity of the problem, but may have introduced some inaccuracy.

References

1. Fröhlich, H.; Proc. Roy. Soc. A160, 230 (1937).
A178, 493 (1942).
A188, 521 (1947).

Seitz, F., Phys. Rev. 76, 1376 (1949).

2. Von Hippel, A.; J. Appl. Phys. 8, 815 (1937)
Phys. Rev. 54, 1096 (1938).

Von Hippel, A. and Alger, R. S., Phys. Rev. 76, 127 (1949).

3. N. Klein in Advances in Electronics and Electron Physics, 26, ed. by L. Maroon (Academic Press, New York 1969) p. 309, (This also provides a recent review of electric breakdown in insulators).

Vermeer, J. Thesis, KEMA (1959).

4. O'dwyer, J. J., J. Appl. Phys. 40, 3887 (1969).

5. Forloni, F. and N. Minnoja, Phys. Stat. Solidi 4, 311 (1964).

6. DiStefano, T. H. and Eastman, D. E. Phys. Rev. Letters, 27, 1560 (1971).

7. Shatzkes, M. and Av-Ron, M., to be published, J. Appl Phys. (May 1974).

8. T. H. DiStefano and D. E. Eastman, Solid State Comm. 9, 2259 (1971).

9. M. Lenzlinger and E. H. Snow, J. Appl. Phys. 40, 278 (1969).

10. Conwell, E. M. "High Field Transport in Semiconductors" Academic Press, N.Y. (1967).

11. Rose, A., "Concepts in Photoconductivity and Allied Problems:, Interscience, N.Y. 1963.

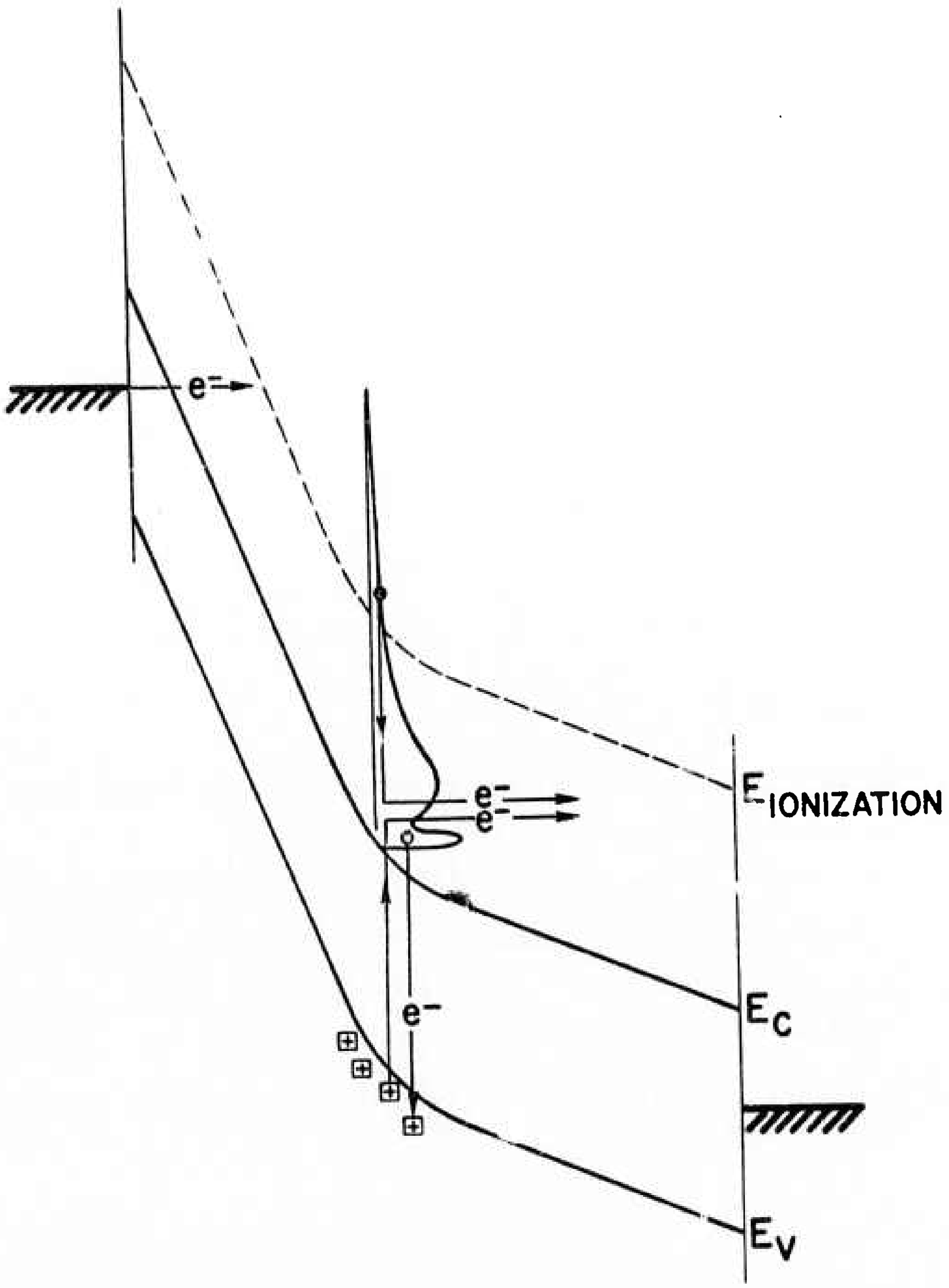

Figure 1: Electrons injected from the cathode lose energy via phonon collisions, so that the electron energy distribution at a position within the insulator will be as shown. Those electrons with kinetic energy larger than the ionization energy undergo impact ionization, losing energy in the process; an electron is excited into the conduction band from the valence band leaving an immobile hole. Electrons recombine with the holes. The positive space charge causes an enhancement of the field at the cathode.

Figure 2: Current density vs applied voltage for a 1000 Å SiO_2 layer. For current densities below the onset of negative resistance, the curve is independent of the value chosen for the ionization mean free path λ_i. In the negative resistance regime variations with λ_i are significant. The breakdown voltage is the maximum applied voltage such that a steady state solution for the current is possible.

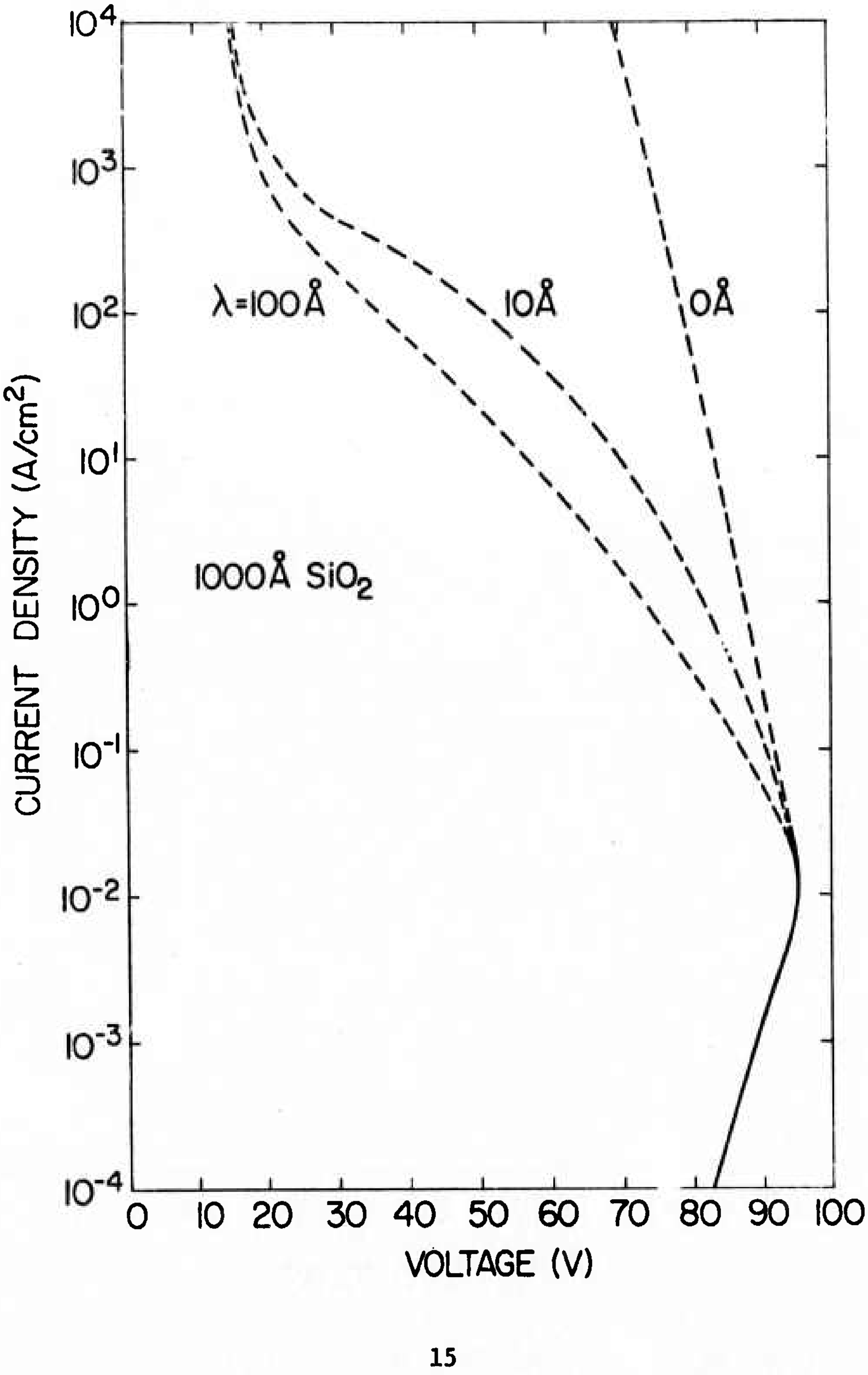

Figure 3: Current density vs applied voltage for two models of electron-hole recombination. In both cases $\lambda_I = 0$, for the Milne model the phonon mean free path $\lambda = 1.34$ Å, while for the Rose model $\lambda = 1.68$ Å. With these choices for λ, the breakdown voltage is the same for both models, though recombination cross sections differ by about a factor of 10^6, the Milne cross section being smaller. This illustrates the extreme insensitivity of the calculation to variations in the recombination cross section.

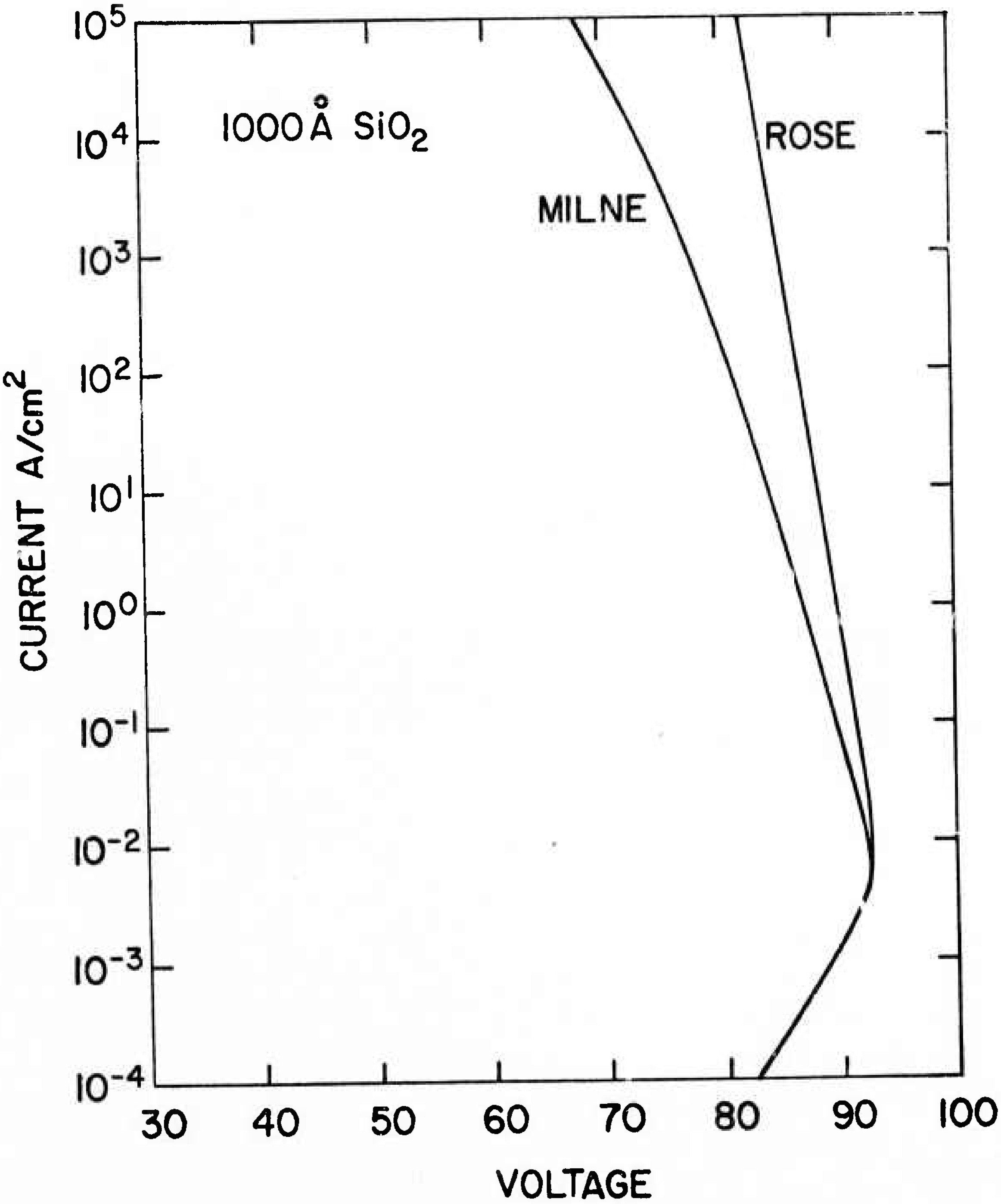

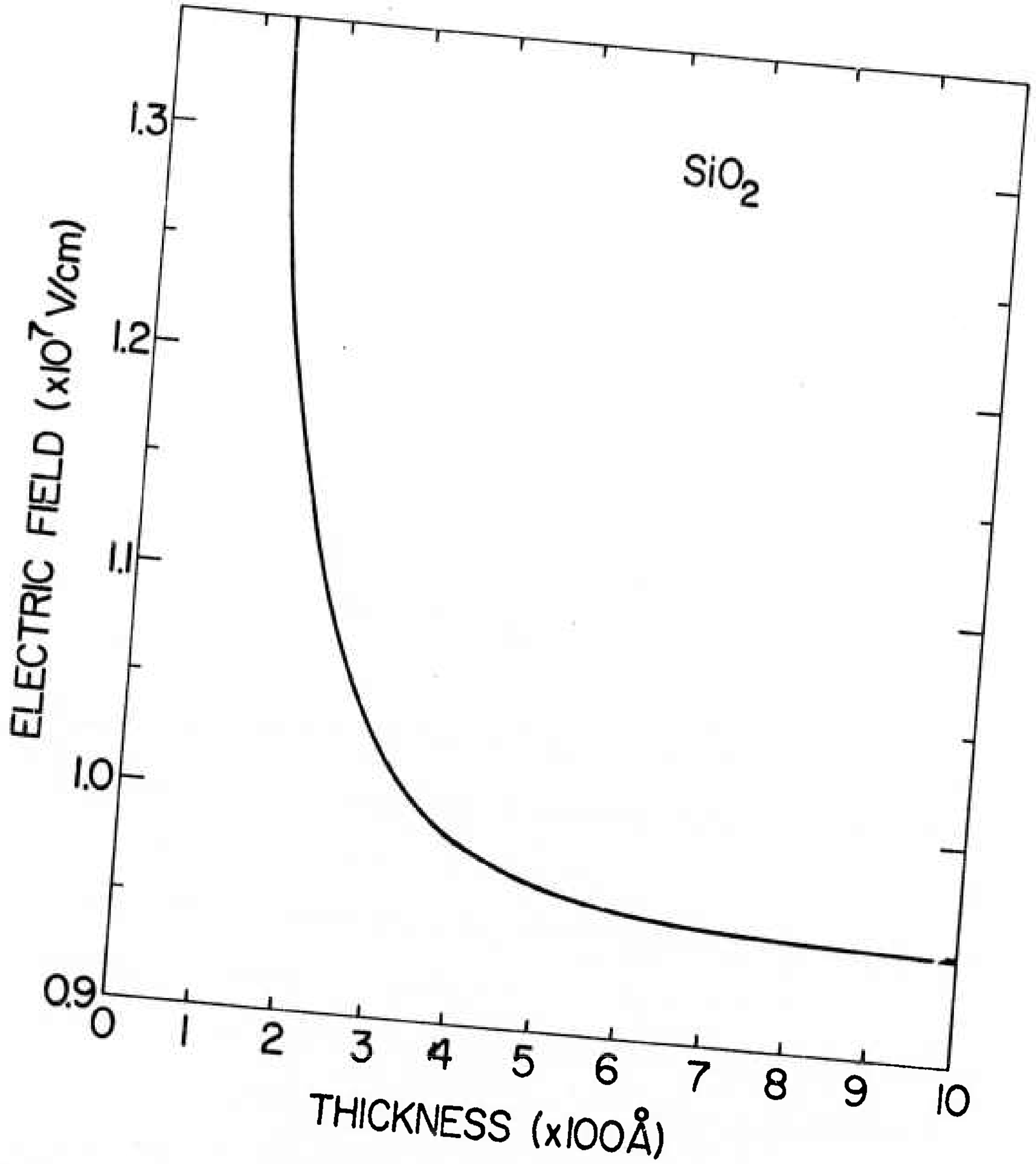

Figure 4: Computed dependence of the average field at breakdown on the thickness of the SiO$_2$ layer. The phonon mean free path is adjusted to give the indicated average field for the 1000 Å layer. The Milne model for recombination is used with $\lambda = 1.34$ Å.

B. PHOSPHORUS PRECIPITATION ON Si/SiO_2 INTERFACES

T. H. DiStefano

Scanning internal photoemission has been used to study the recently discovered phenomonon[1,2] that phosphorus is found in a thin layer on the oxide side of a $Si-SiO_2$ interface formed by the oxidation of phosphous doped silicon. It is well known that the silicon surface of each interface has an enhanced phosphorus concentration. The phosphorus found on the interface is different in that it comprises a large fraction of a monolayer of phosphorus in a layer which is 10 Å or less in thickness. By using scanning internal photoemission, we have been able to examine the distribution of phosphorus on the interface. We have found islands of phosphorus, from 1 to 10 microns in diameter or even larger in some cases, distribution across the interface. The island size depends upon the concentration of phosphorus in the substrate.

The interfaces which were studied were prepared by thermal oxidation of the (100) surface of phosphorus doped silicon. The oxidation was performed by the standard dry-wet-dry technique at 1100°C, to obtain a film of SiO_2 to a thickness of 1000 Å. Before oxidation, the silicon surface was phosphorus doped by diffusion to a depth of ∿ 2 microns; the surface of the silicon was cleaned after the phosphorus diffusion by a surface etch procedure. The photoemission measurements were performed on a series of interfaces grown on silicon with a range of phosphous doping levels.

The photoemission images are shown in Figs. 1-4, where the field of view is 250 microns by 250 microns. Interfaces grown on a silicon with a doping level of about 5×10^{19} P/cm^2, shown in Figs. 1-2, show phosphous islands about 10 microns in diameter. For a substrate doping level of about 2×10^{19} P.cm^3, the phosphous islands are much smaller and further apart as seen in Figs. 3-4. On interfaces grown on less heavily doped silicon show few of these phosphous islands, while those grown on silicon doped to lo^{20}P/cm^3 are completely covered with the phosphorus precipitate. The influence of the phosphorus doping level is summarized in Fig. 5, which shows the photocurrent produced by light at 3250 Å for interfaces grown on silicon with a range of phosphorus doping. It is seen that the average photocurrent drops rapidly with increasing phosphorus up to a level of 10^{20} P/cm^3, at which point the photocurrent disappears completely. This phosphorus level corresponds to a concentration of 5×10^{-4} P/cm^2 on the interface, if it is assumed that all of the phosphorus in the oxidized layer of silicon has segregated at the Si-SiO$_2$ interface.

References:

1. T. H. DiStefano and J. M. Viggiano, IBM J. Res. and Develop. 18, 94, (1974).

2. N. Chan and Y. van der Meulen, to be published.

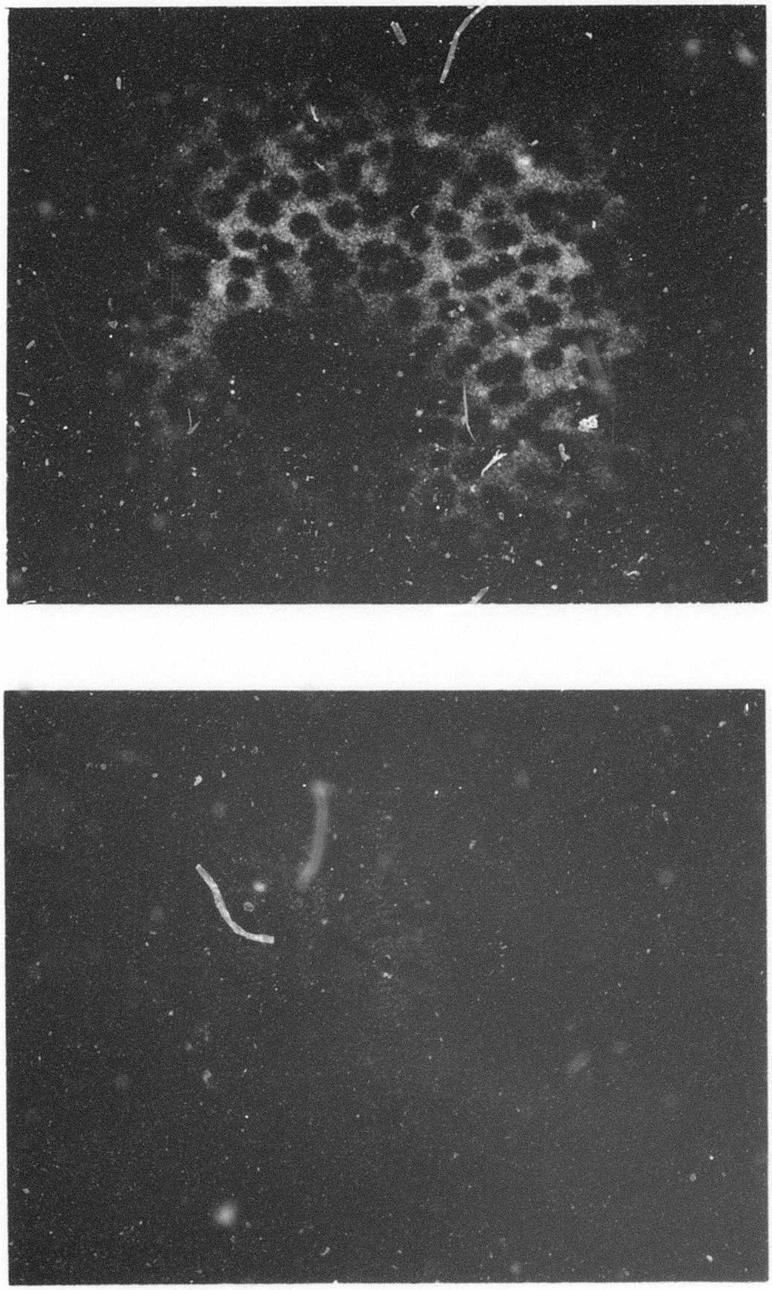

Figure 1 and 2: Scanning Internal Photoemission maps of an Si-SiO_2 interface gronw on silicon (100) with a surface phosphorus doping level of 5×10^{19} P/cm^3.

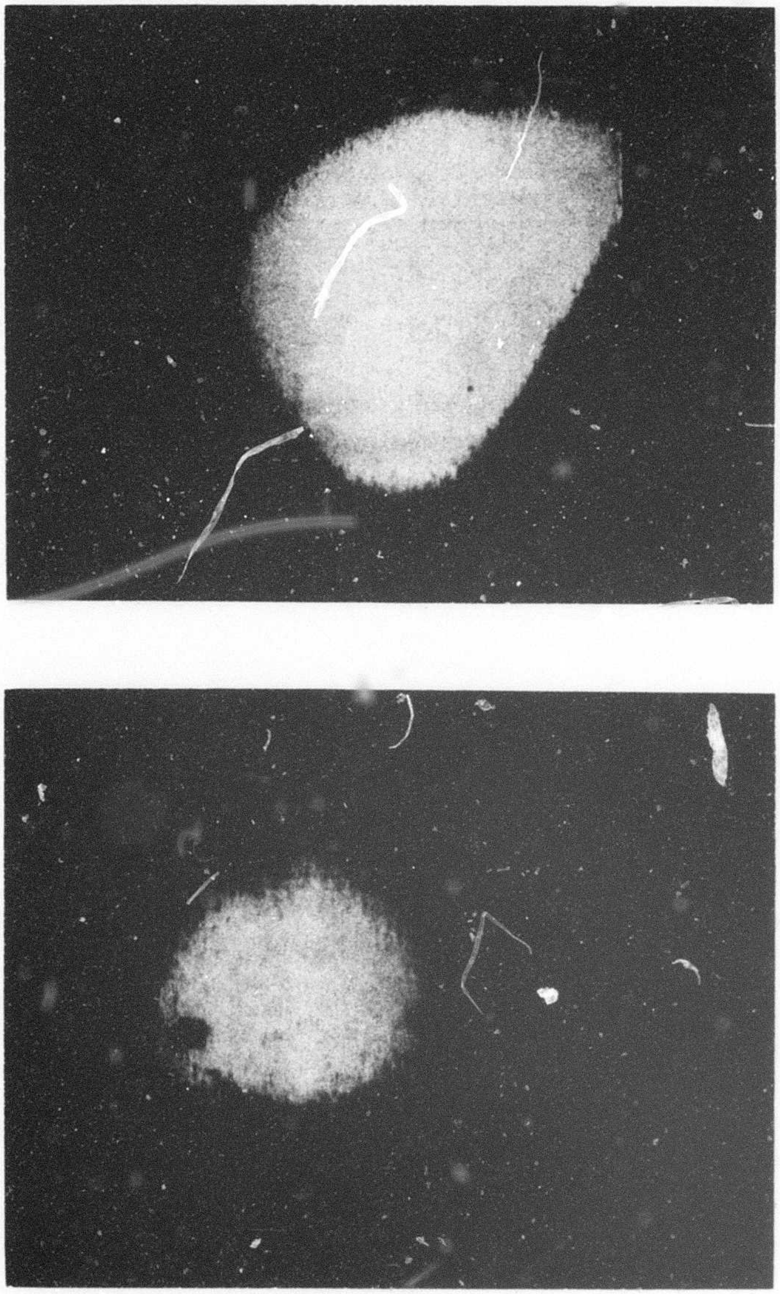

Figure 3 and 4: Scanning Internal Photoemission maps of a Si-SiO$_2$ interface grown on silicon (100) with a surface phosphorus doping level of 2 x 10^{19} P/cm^3.

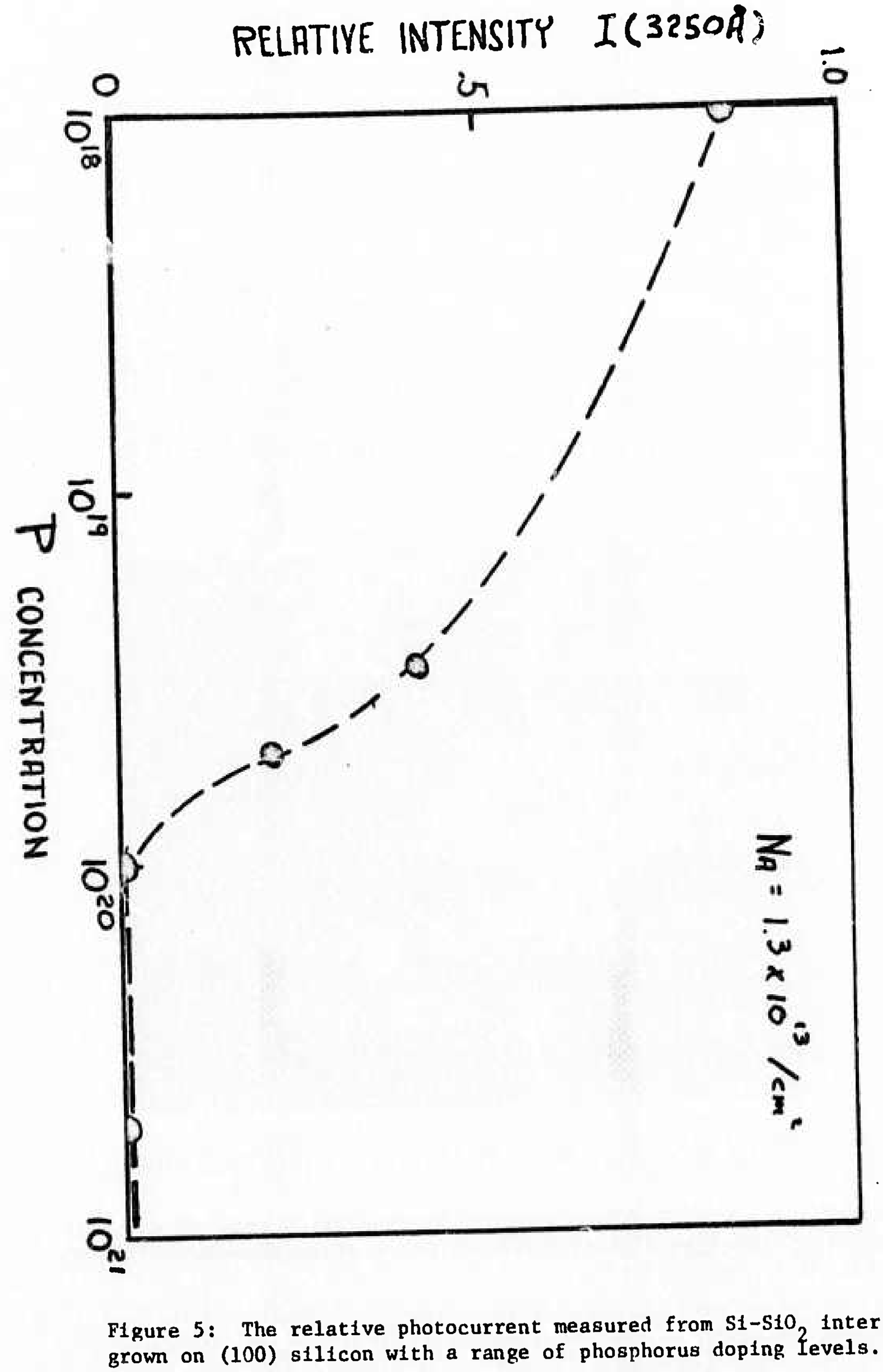

Figure 5: The relative photocurrent measured from Si-SiO_2 interfaces grown on (100) silicon with a range of phosphorus doping levels.

II. BAND STRUCTURE AND SWITCHING IN INSULATORS

From our theoretical work on dielectric breakdown mechanisms, it has become apparent that more information is necessary to understand the role of holes in the SiO_2 formed by impact ionization or by radiation. Accumulation of positive charge causes increased field at the cathode and increased carrier injection. The stability of the holes in terms of their mobility is key to the predictions of the theory. To help gain needed insight into hole mobility, it is desireable to ascertain the valence band width. To do this, the effects of crystal field splitting must be minimized. This was accomplished by measuring the reflectivity of the allotropes of SiO_2 characterized by different angles of the Si-O-Si bond: α quartz, amorphous quartz, cristobalite. The latter case should not show crystal field splitting. The optical transitions giving rise to the reflectivity results indicated a valence band width of about 1 eV. This finite width implies that hole conduction is possible, but the small width means that any lattice defect, such as unbridged oxygen, will induce trapping of any holes in the valence band (Anderson localization).

The second paper deals with change in resistance state of $Ge_{15}Te_{85}$ films by switching between three different structures. The highest resistance state is found for the completely amorphous film. When switching to a lower resistance state crystallites of Te are formed in a still amorphous matrix. The lowest reistance state involves a second switch in which the matrix crystallizes to GeTe. Switching between the lowest two states is readily accomplished. However, by simultaneously observing the structural changes occurring during the switching process by transmission electron microscopy it can be concluded that permanent degradation of the film increases until failure ultimately takes place. This seems typical of other switchable materials we have investigated in the past such as Nb_2O_5 where atomic rearrangement accompanies the switching process.

A. OPTICAL PROPERTIES OF ALLOTROPIC FORMS OF SiO_2

T. H. DiStefano and P. K. Roy

Until recently, little has been reported about the electronic structure of SiO_2 which determines several physical, optical and dielectric properties. Knowledge of the valence band (VB) structure is important to current studies of radiation damage, electronic structure of various defects, and properties of Si (or metal)-SiO_2 interfaces. Optical properties (ultraviolet reflectance spectra from 8 to 13 eV in the present case) for different allotropes of SiO_2 will give -

(a) detailed information about the structure of the relatively unknown VB edge.

(b) variations of optical and dielectric properties as a function of Si-O-Si bond angle, Θ. As we know Θ varies from 120° (coesite) to 180° (for cristobalite or tridymite) with crystalline and amorphous quartz having bond angles of 144° and 150°, respectively.

(c) The width of the top of the VB (ΔE, Fig. 2), which plays a very important role in determining the mobility of the holes created when SiO_2 is subjected to an ionizing radiation.

The structure of amorphous SiO_2 can be understood in terms of β-crystobalite, in which the SiO_4 tetrahedra occupying the points of the diamond lattice are connected by straight Si-O-Si chains. Oxygen in this lattice occupies the sites of D_{3d} symmetry shown in Fig. 1 (a). In the amorphous SiO_2, the Si-O-Si chain is bent to an angle of about 150°. The electronic levels in the amorphous structure are conveniently described with the $O^{--}2S^2 2p^6$ orbitals as a basis. As displayed in Fig. 1(b), the s and p orbitals of the O^{--} ion in free space are separated by 14.9 eV. In the D_{3d} symmetry of β-crystobalite, the $2p^6$ degeneracy is split to produce two nonbonding orbitals (Γ_6) which are perpendicular to the Si-O-Si chain, and one bonding orbital (Γ_3) which links the Si and O centers. The s orbitals remain as the Γ_1 level in D_{3d}. In going to the amorphous structure, the electronic levels found in D_{3d} broaden into bands as shown in Fig. 1. Also, by symmetry considerations, the Γ_6 level is shown to split into two nonbonding bands, corresponding to nonbonding orbitals which lie perpendicular to and parallel to a plane determined by the Si-O-Si chain. The two nonbonding bands, the bonding bands, and the deep-lying s band, described in terms of an O^{--}-ion basis, are equivalent to those found theoretically by Reilly who used hybrid Si orbitals and atomic O orbitals as a basis. Reilly's determination of the energy levels of SiO_2 using linear combinations of atomic and molecular orbitals shows two nonbonding levels at the valence-band edge, split by about 2 eV, with a bonding level at about 12 eV below the valence-band edge. The oxygen 2s level was placed at about 24 eV below the band edge.

Details of the emission spectra from SiO_2 can be identified in terms of bands in Fig. 1(b). The two peaks at the valence-band edge have a total width at half-maximum of only 3.2 eV, presumably because of the small overlap between the nonbonding orbitals. The bonding band, seen to extend from about -5.5 to -11.2 eV in the emission spectra, is considerably broader than either of the nonbonding bands because of the larger overlap of bonding orbitals. The conduction band, which begins at 9.0 eV above the top of the valence band, includes the Si-O antibonding orbitals.

Figure 2 summarizes schematically the electronic structure of SiO_2 and hence the expected optical transitions from the two nonbonding orbitals in the VB to the unfilled 3d level of Si, which can be probed by no reflectance measurements. For bond angles less than 180°, due to crystal field effects the degeneracy of p-orbitals will be removed and the bottom nonbonding orbital will lower its energy by s - p orbital mixing (Fig. 2a). The VB width, ΔE, shown in Fig. 2b due to crystal field splitting alone will have a functional dependence of Θ as shown in Fig. 2c. Figure 2 summarizes the expected optical and dielectric properties of SiO_2 resulting from the electronic transitions from the two top nonbonding orbitals of the VB mainly to the unfilled Si 3d-level in the CB as a function of Θ. The transitions mainly control ΔE if it came only due to crystal field effects. The uv reflectance spectra should probe all such transitions and their dependence on Θ.

Coesite was not studied due to the unavailability of this particular allotrope of SiO_2 with sufficient macroscopic size and optically good surface for reflectivity studies. Synthetic cristobalite samples were preposed by soaking amorphous quartz discs at 1400°C for 90 hours followed by a second soaking at 865°C for 30 hours before furnace quenching to room temperature. On the basis of the twelve strongest reflections found by x-ray diffraction, samples were identified as 100 percent α-cristobalite with a <101> texture. Tridymite was not independently studied as the bond angle, Θ, for this allotrope is the same as that of cristobalite. The fused quartz (optical grade) and the Z-cut α-quartz samples were used to represent amorphous and crystalline allotropes, respectively. For reflectivity measurements a McPhearson-225 type monochrometer was used which is capable of generating uv light in the energy range 0-15 eV. Light from a thoriated tungsten filament using a glow discharge in hydrogen gas was used as the source of light. The light goes through concave gratings before coming to the exit slit. Optics from the exit slit to the sample holder assembly, which is vacuum sealed to the monochrometer, is shown in Fig. 3 for the reflected light configuration. The incident light intensity configuration was attained by rotating the mirror 90° about the axis perpendicular to the plane of the paper. Both the incident and the reflected intensity were detected by the sodium salicylate window of the photomultiplier tube. In these particular optical arrangements, in either the reflected or incident light configurations, the pencil of light hits about the same location of the mirror only once, thus minimizing errors in the reflectivity data.

Figure 4 shows the reflectivity data taken at 0.05 eV intervals. The amorphous SiO_2 shows two distinct peaks located at 10.3 and 11.55 eV, respectively, corresponding to the electronic transitions from the two nonbonding orbitals of the VB edge mainly to the unfilled Si d-level in the CB. The width of the VB edge ΔE, is found to be 1.25 eV. The reflectance spectra for the crystalline quartz was strikingly similar, as observed by others previously, except that the first peak occurring at 10.25 eV is much sharper and that in the second peak, occurring at 10.55 eV, there are considerable fine structures. This is possibly due to other inter-band and/or intraband transitions from the VB edge to other allowed transitions to the bottom of the CB. The results for crystobalite are somewhat unusual in that corresponding peaks are collapsed around 10.7 eV to a twin peak occurring at 10.35 and 10.9 eV, respectively, with additional fine structures.

In spite of the drastic change in Θ, reflectance spectra of the three allotropes are relatively insensitive to Θ. In addition, if the width of the VB edge were determined by the crystal field effects alone, ΔE would have collapsed to zero for cristobalite and a single peak would be expected, which was not the case. This indicates that ΔE is not as narrow as we previously thought and that the band effects due to the overlap of next-nearest neighbor oxygen-oxygen orbitals is rather high in the crystobalite lattice.

Kramer-Kronig analyses were made on the reflectivity data to find the functional dependence of dielectric (ε_1, ε_2) and other derived optical (n, k) properties on Θ. ε_1 and ε_2 are the real and imaginary part of the frequency-dependent dielectric function, $\varepsilon(w)$ and n and k are, respectively, the index of refraction and extinction coefficient. ($\varepsilon = \varepsilon_1 + i\varepsilon_2$; $(n + ik)^2 = \varepsilon_1 + i\varepsilon_2$) Figures 5 and 6 show the variations of (ε_1, ε_2) and (n, k), respectively, as a function of photon energy for all the three stated allotropes. They show similar variations, as seen in the raw reflectivity data, except that the fine structures are amplified. The variations of ε_2 as a function of photon energy from Fig. 5, below the absorption edge, can be best fitted to a parabola and the results are shown in Fig. 7. The functional dependence of $\sqrt{\varepsilon_2}$ near the VB edge on the photon energy locates exactly the VB edge, which was found to be 9.05.9.1 and 9.25 eV for cristobalite, amorphous and crystalline quartz, respectively.

The reflectance spectra are relatively similar for cristobalite, amorphous and crystalline quartz. This leads us to believe a simple model based on the oscillations from an unhybridized O^{--}p orbitals to the unfilled Si 3d-level in the CB.

The width of the VB edge (ΔE) is comparable for all three allotropes and hence the band broadening effects due to the overlap of two next-nearest-neighbor oxygen orbitals is high enough to give a finite width for cristobalite ($\theta = 180°$), where there is no crystal field effects.

ΔE is of the order of 1 eV which is broader than previously thought; however, it is narrow enough to cause localization and trapping of holes in an SiO_2 lattice, relatively defect free, when SiO_2 is subject to an ionizing radiation.

Figure 1: Structure and energy levels of SiO_2. (a) The line Si-O-Si in cubic SiO_2 is straight, while this line in amorphous SiO_2 is bent to about 150°. (b) Energy levels shown are O^{--} in free space, O^{--} in the group D_{3d}, and the valence band of amorphous SiO_2.

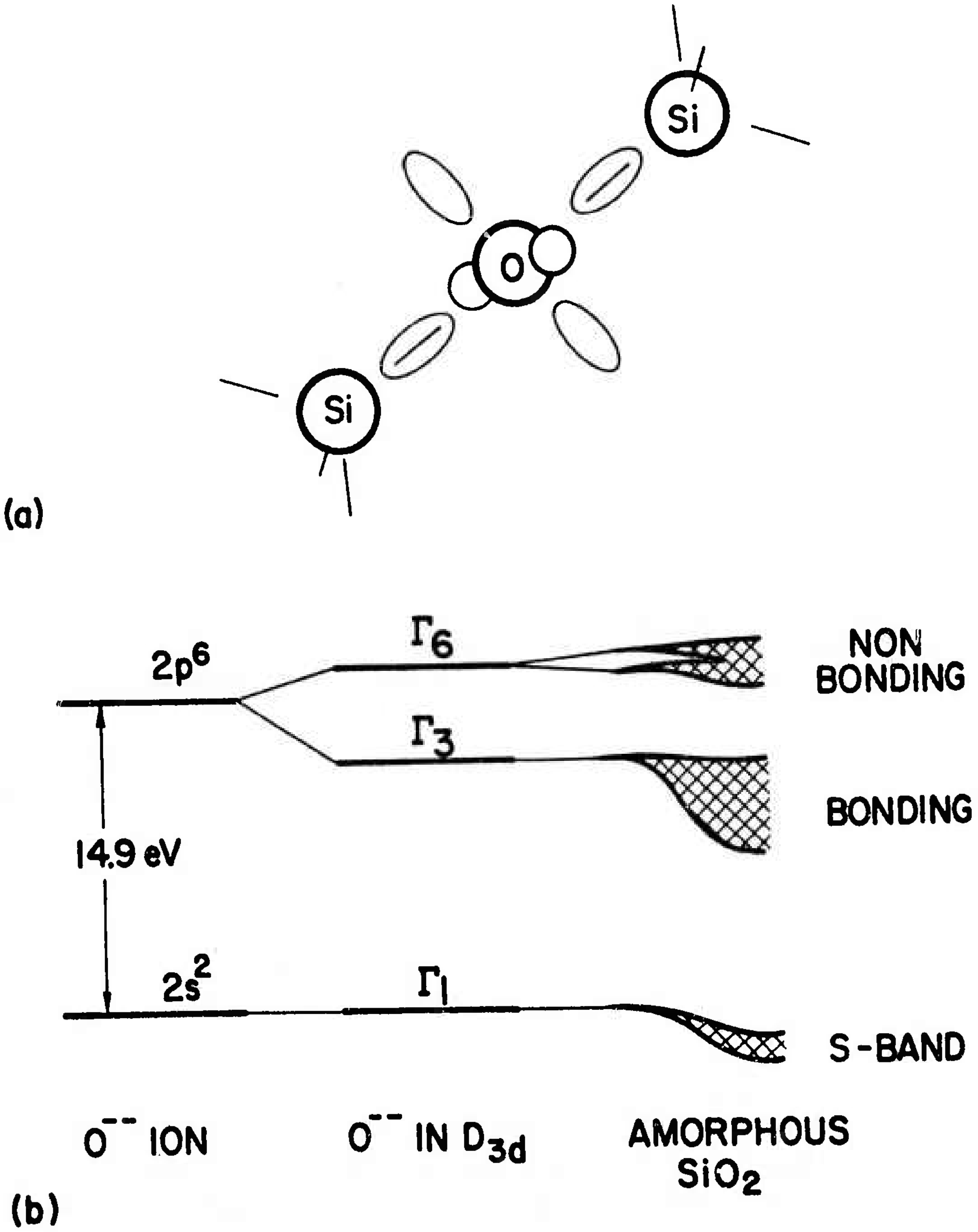

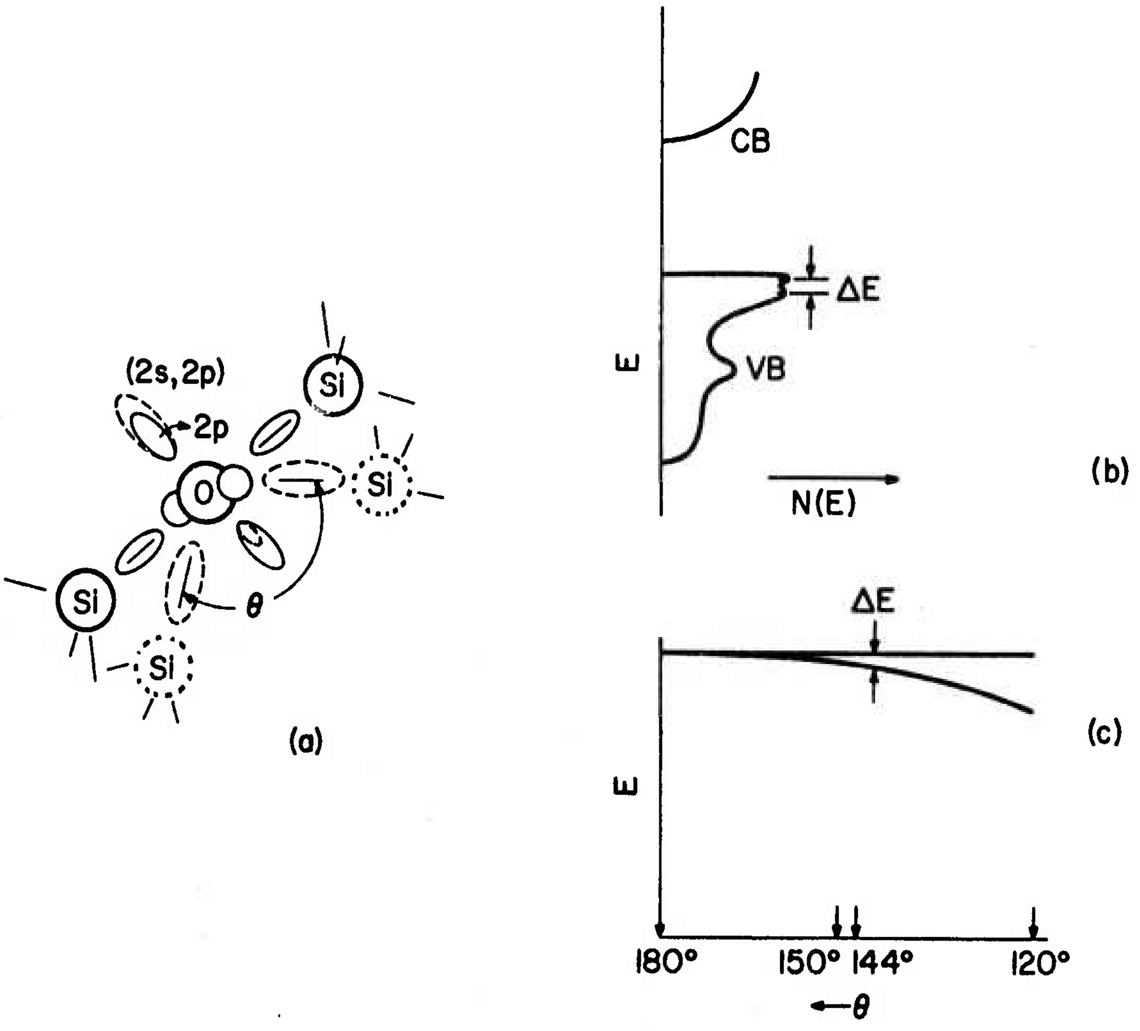

Figure 2: Electronic structure and the valence band (VB) edge in SiO$_2$[22] (a) For θ < 180°, the mixing of lower nonbonding 2p^6 orbital with 2s orbital due to crystal field effects (b) the top of the VB edge and its width, ΔE (c) the functional dependence of location of VB edge and ΔE on Θ.

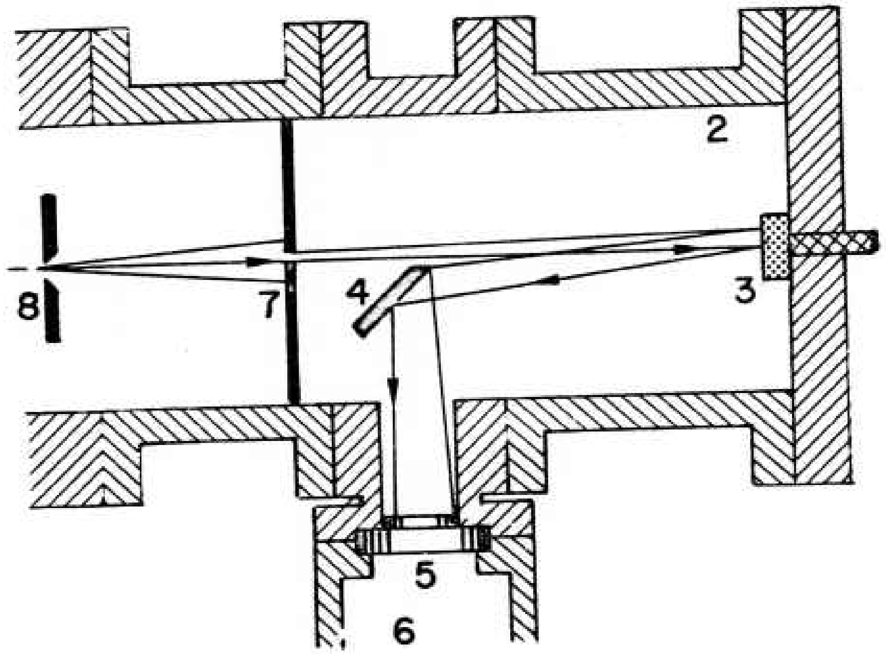

Figure 3: Reflectivity apparatus, schematic (1,2,3) sample holder assembly, (4) mirror, (5,6) photomultiplier detector assembly, (7,8) slit width adjustment assembly.

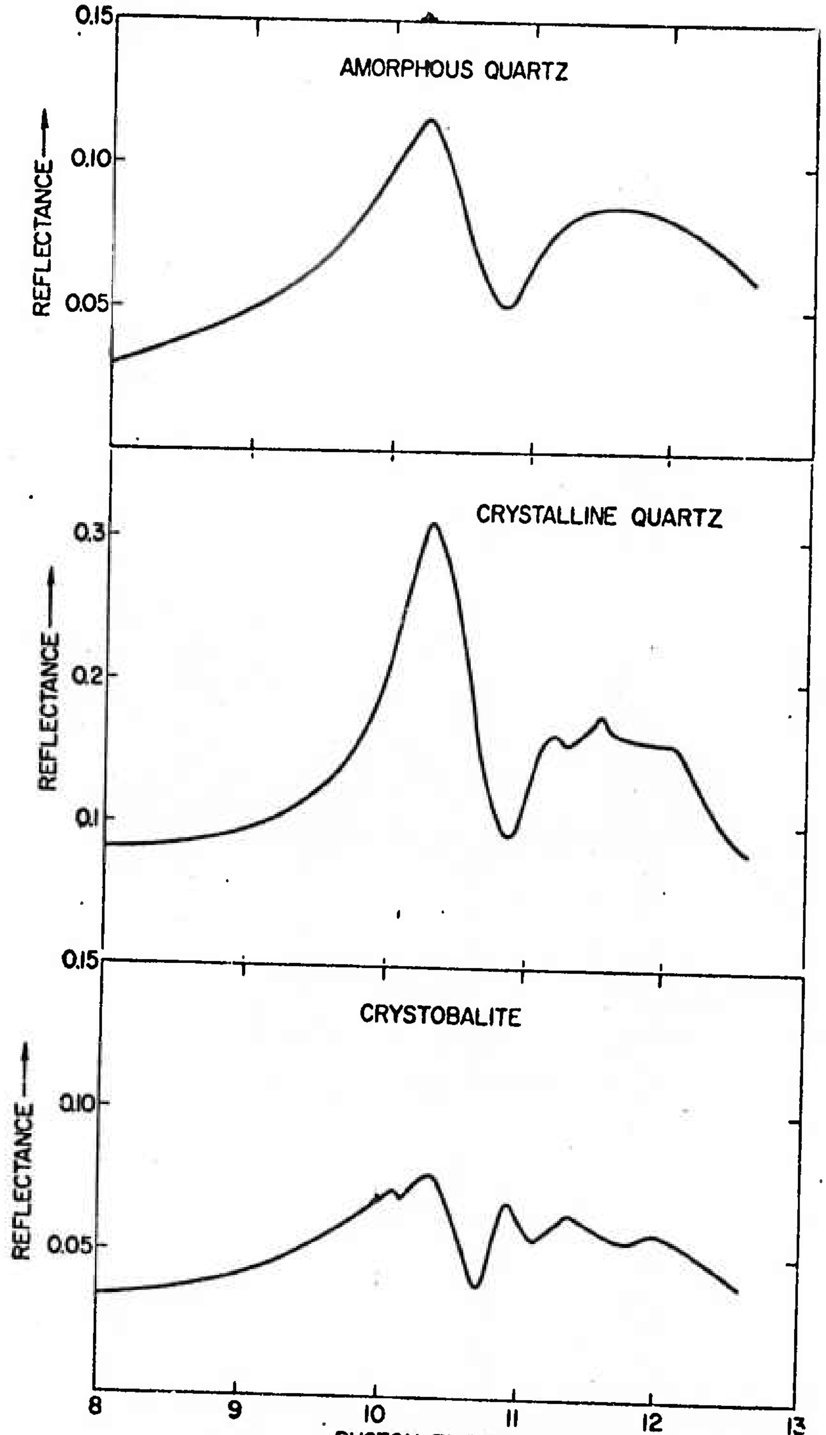

Figure 4: The uv reflectance vs photon energy.

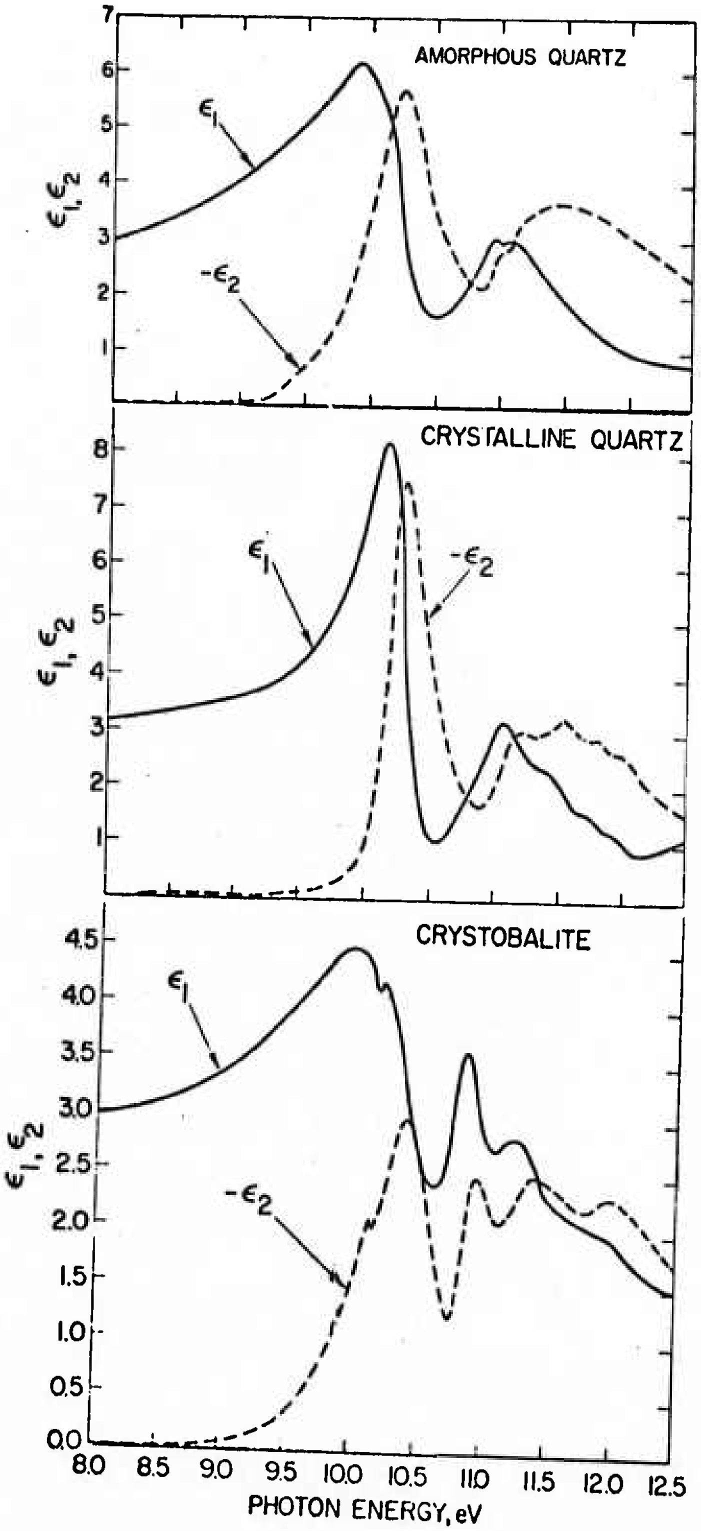

Figure 5: ε_1,, ε_2 vs photon energy.

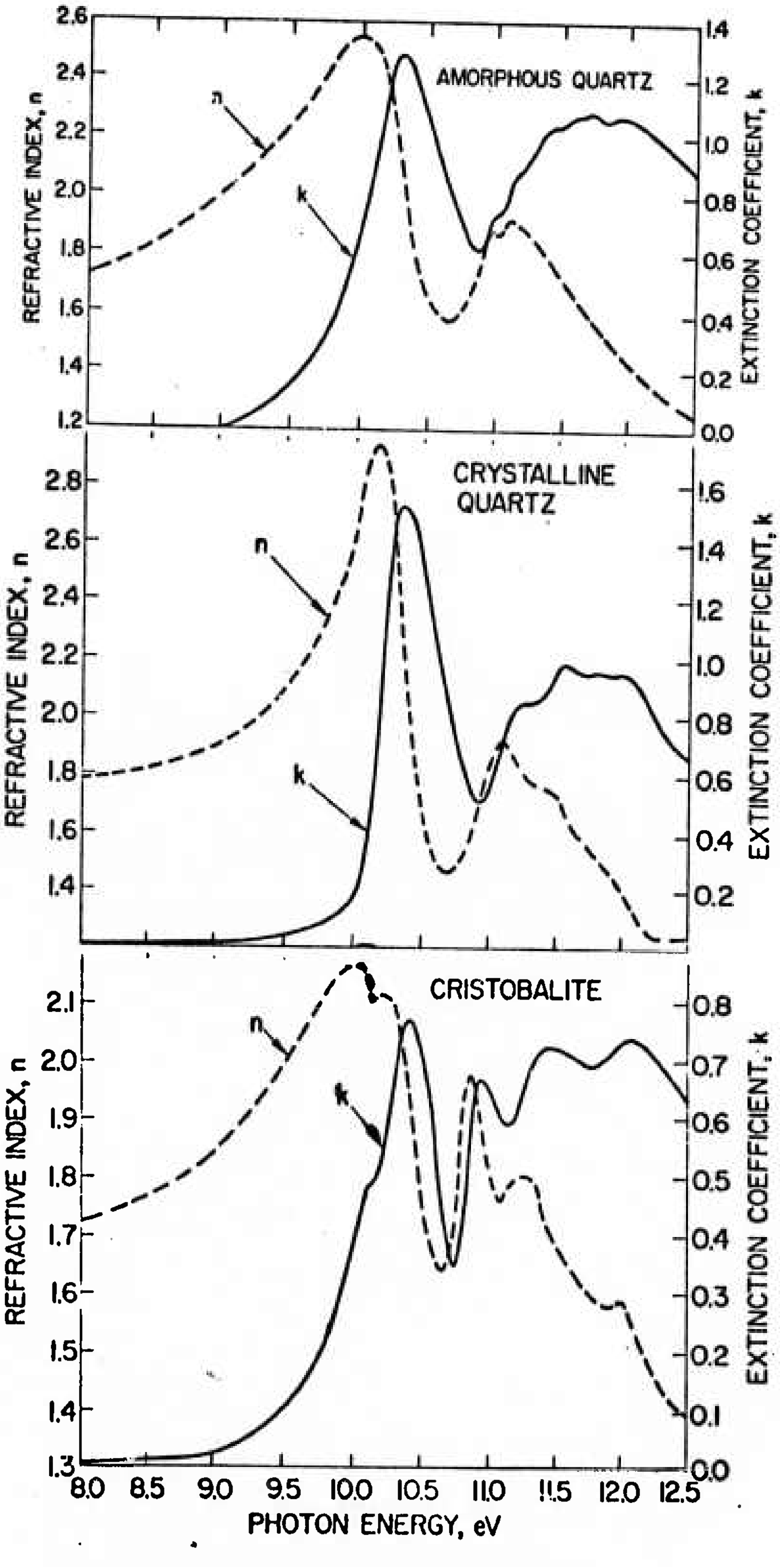

Figure 6: n, k vs photon energy.

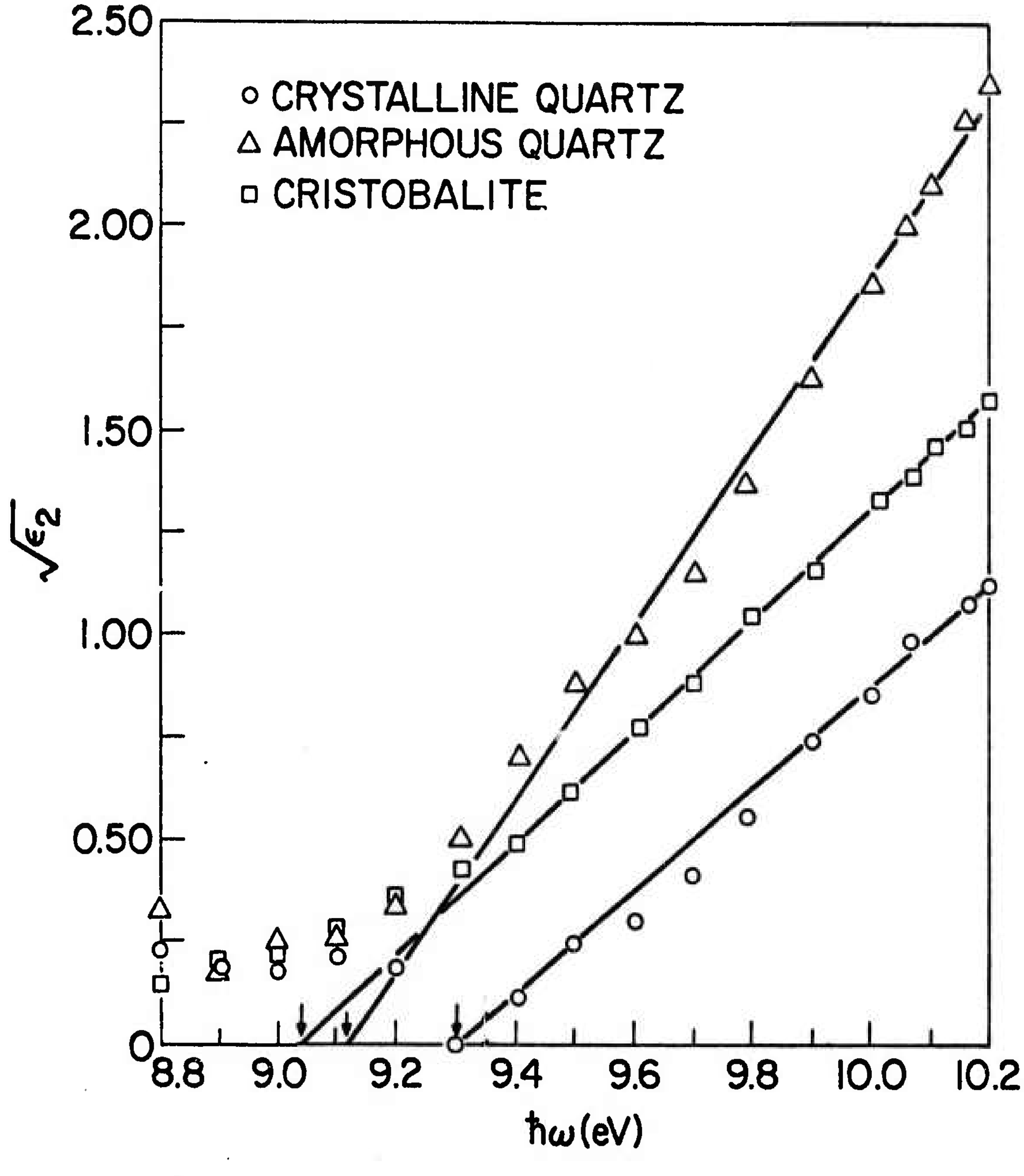

Figure 7: $\sqrt{\epsilon_2}$ vs photon energy.

B. STRUCTURAL TRANSFORMATIONS AS OBSERVED BY TEM DURING ELECTRICAL SWITCHING IN AMORPHOUS Ge-Te

R. B. Laibowitz, S. R. Herd and P. Chaudhari

ABSTRACT: Structural transformations were induced in thin films of amorphous Ge-Te by an applied voltage while the sample was simultaneously viewed via transmission electron microscopy. Three resistance states were observed, the highest for the completely amorphous phase, and the lower two for states consisting of crystalline Te in both an amorphous material and in crystalline GeTe. Switching between the lower two states can be accomplished, but with increasing material degradation. In situ electron diffraction was used to identify the various phases.

When thin films of amorphous Ge-Te are sandwiched between conducting electrodes and biased, electrical switching between two resistance states occurs (Ovshinsky 1968). In general, two distinct bistable resistance characteristics have been observed: one in which the resistance state can be maintained at zero bias (memory state) and a second in which a holding voltage is necessary to maintain the particular resistance. While work has been done attempting to understand these properties in Ge-Te and other amorphous materials (Bosnell and Thomas 1973), the physical mechanisms responsible for the conductivity changes remain as yet unresolved. This is especially true of the morphological transformations that occur in these systems. In this letter, we report on the results of an investigation in which we determined the microscopic structural changes in the amorphous $Ge_{15}Te_{85}$ during switching and related these changes to the presence and behavior of the memory state. The technique we used was to directly view the amorphous material via high resolution transmission electron microscopy (TEM) while simultaneously taking I-V curves which showed the switching behavior (Chaudhari and Laibowitz 1972; Laibowitz, Chaudhari, Herd and Mader 1973). In addition, in situ electron diffraction was used to identify the structure after phase changes were observed.

The experimental set-up will be briefly reviewed here; a more complete discussion of the sample configuration can be found in our earlier report (Chaudhari and Laibowitz 1972). Basically, two closely spaced metal electrodes were fabricated on the surface of an oxidized Si wafer by electron beam techniques (Hatzakis and Broers 1971). The width of the gap between the two electrodes could be varied from about 0.1μ to several microns. Amorphous Ge-Te of approximately $Ge_{15}Te_{85}$ composition was then coevaporated from separate sources onto this sample, filling the gap. The substrate beneath the gap was then selectively back-etched until the remaining SiO_2 with the Ge-Te on top was transparent to 100 KeV electrons used in the microscope. In general, the thickness of the Ge-Te was about 0.1μ or less with a residual SiO_2 thickness of about 0.02μ. Leads were then connected to the metal electrodes (Al) and the sample mounted in the microscope. Either ramp or pulsed biases could be applied to the sample by external sources and the response of the sample was monitored on an oscilloscope.

When a bias was first applied across the gap, i.e., across the Ge-Te, a very high resistance state was obtained. Upon increasing the voltage, a partial breakdown (or forming) occurred resulting in a low resistance state. This low resistance state is caused by conduction through crystalline filaments (Chaudhari and Laibowitz 1972) which bridge the gap as shown in Fig. 1. However, this type filament could only be observed in thicker ($\gtrsim$ 0.1μ) Ge-Te films which allowed visual observation but were too thick for electron diffraction.

Subsequent measurements on thinner (0.06μ) Ge-Te films allowed analysis by electron diffraction and are shown in Figs. 2a and 2b. Again, after the low resistance state was obtained, we found crystallization, although the morphology of the crystals in the thin films is somewhat different. The speckled regions of Figs. 2a and 2b show crystalline Te particles in an amorphous Ge-Te matrix which are similar to the crystals observed after the first forming took place. Upon applying a high current pulse, the Te redissolves and the material becomes amorphous again, i.e., the material attempts to return to its initial high resistivity state. Some damage usually occurs in these films during switching with a high current pulse due to material flow.

Figure 2a shows the sample in its lowest resistance state after a few switching cycles. We find a band of small Te crystals as observed after the initial forming. In addition, near the top of Fig. 2a where the material thickened due to flow during the previous resetting, we find two kinds of crystallization. Conduction occurs through both Te dendrites in amorphous Ge-Te (right marker) and Te in crystalline GeTe (left marker). Figure 3 shows the selected area diffraction pattern and micrographs of this region at a higher magnification. Most of the spotty rings in the selected area diffraction pattern (Fig. 3a) are due to randomly oriented Te crystals (hex., $a_o = 4.46$ Å; $c_o = 5.93$ Å). The short arced spot marked by a circle in the diffraction pattern is due to the <200> reflection of GeTe. A dark field micrograph (Fig. 3b) taken with this reflection shows that the Te crystals visible in bright field in Fig. 3c are embedded in essentially a single crystal of GeTe. There are indications that the GeTe is in the rhombohedral form ($a = 5.98$ Å) ($\alpha = 88.35°$), (Chopra and Bahl 1969) however, positive distinction from the cubic phase ($a = 5.86$ Å) is difficult in this case.

Subsequent switching with a high current pulse rendered this same area amorphous again as shown in Fig. 2b and simultaneously the sample returned to a higher resistance state. Temperatures reached during switching are thus high enough to melt both crystal phases and quench the melt back into an amorphous solid. Again, material flow took place during this resetting operation indicated by the thick ridge of amorphous material in the top section of Fig. 2b. Also visible is a sharp demarkation line where the temperature was not sufficient to redissolve the small Te crystals in the lower half of the micrograph.

Thus, our experiment which combines transmission electron microscopy with electrical switching has shown that three conductivity states can be produced in $Ge_{15}Te_{85}$ and that these three states have specific morphologies associated with them. The completely amorphous phase has the highest resistance while the combination of Te crystallites in an amorphous background has a lower resistance. The lowest resistance state is achieved with both crystalline GeTe and crystalline Te in the conducting filamentary region. While it is possible to cycle (or switch several times between these resistance states, the damage in these very thin films due to material flow usually increases leading to eventual burn out.

REFERENCES

Bosnell, J. R. and Thomas, C. B., 1973, Phil. Mag., 27, 665

Chaudhari, P. and Laibowitz, R. B., 1972, Thin Solid Films, 12, 239.

Chopra, K. L. and Bahl, S. K., 1969, J. Appl. Phys. 40, 4171.

Hatzakis, M. and Broers, A. N., 1971, Proc. of the 11th Symposium on Electron, Ion and Laser Beam Tech., Boulder

Laibowitz, R. B., Chaudhari, P., Herd, S. R., and Mader, S., 1973, Bull. Am. Phys. Soc., 18, 454.

Ovshinsky, S. R. 1968, Phys. Rev. Lett. 21, 1450.

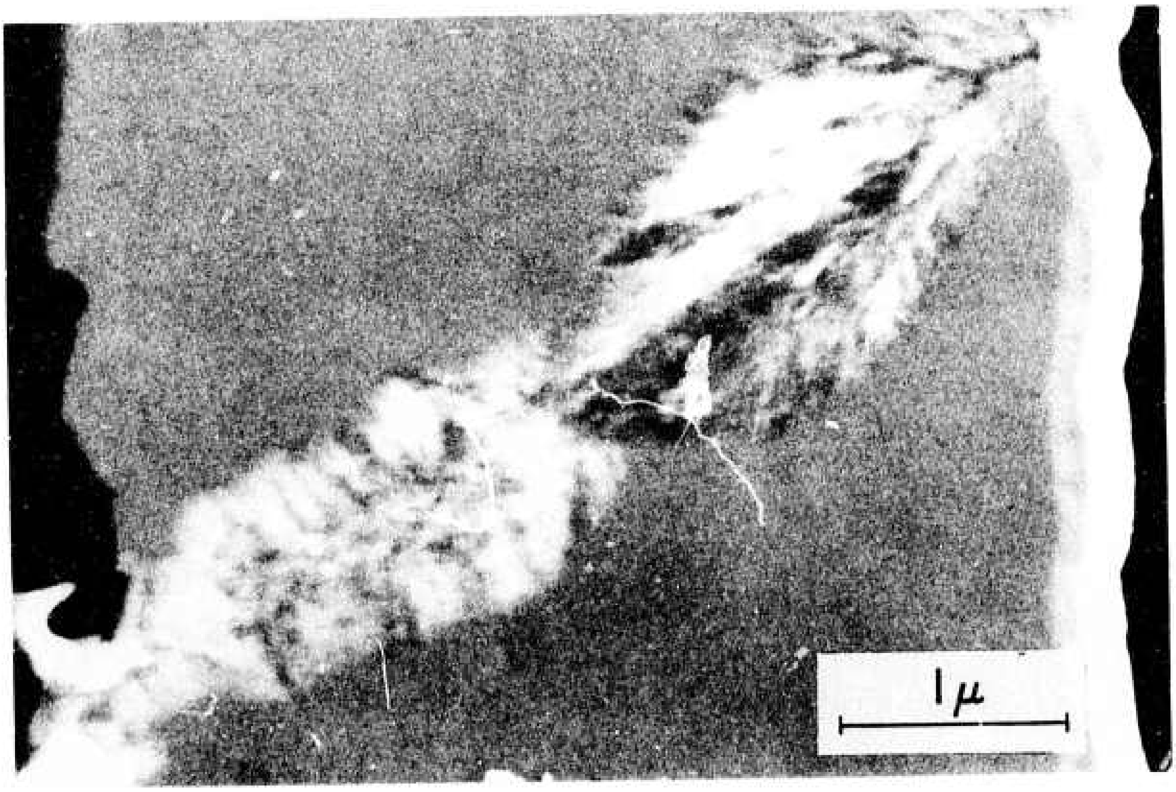

Figure 1: Crystalline filament formed in thick (≥0.1μ) amorphous Ge-Te matrix 30.000 x Mag.

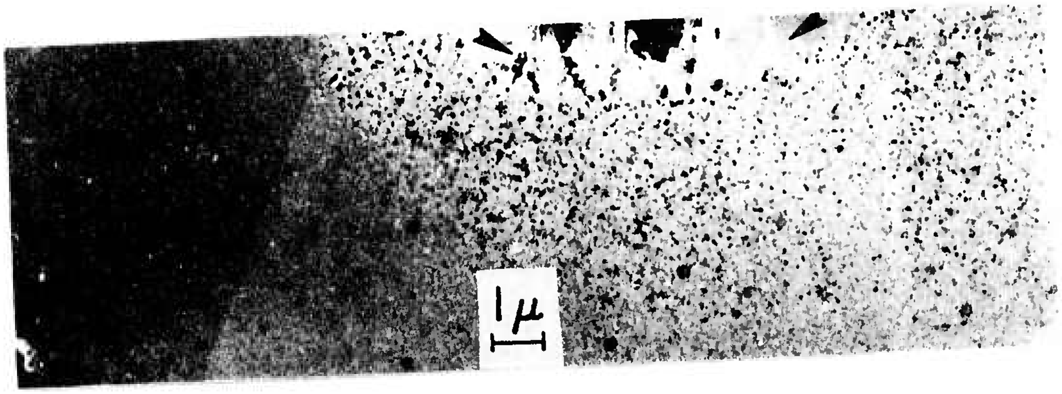

Figure 2a: Crystallization of Te in amorphous Ge-Te matrix and Te imbedded in crystalline GeTe after a few switching cycles. Film thickness - 0.06μ. Lowest resistance state Mag: 6500

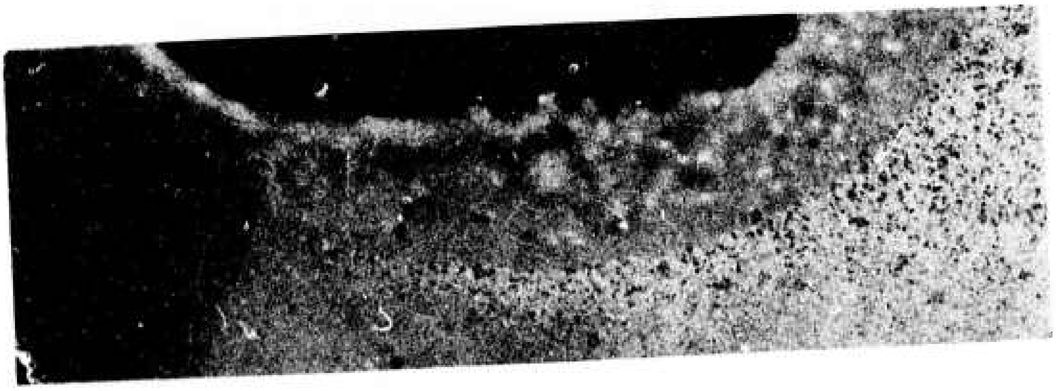

Figure 2b: Same area as Fig. 2a after high current pulse amorphized material.
High resistance state Mag: 6500x

Figure 3a: Selected area diffraction of crystalline Te and GeTe.

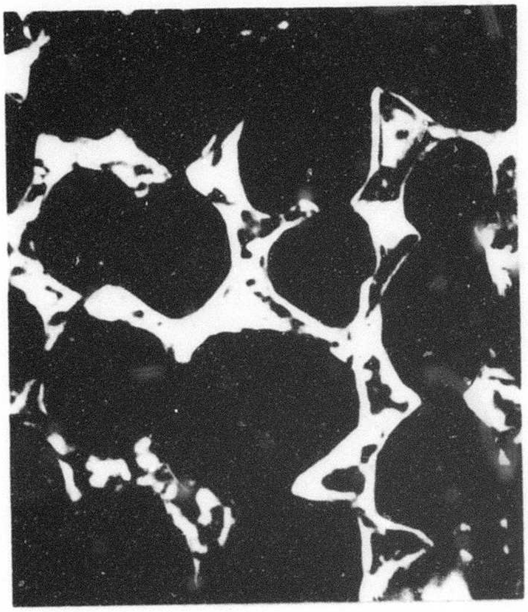

Figure 3b: Dark field mircograph of GeTe crystal taken with <200> reflection as indicated in Fig. 3a Mag: 200,000 x

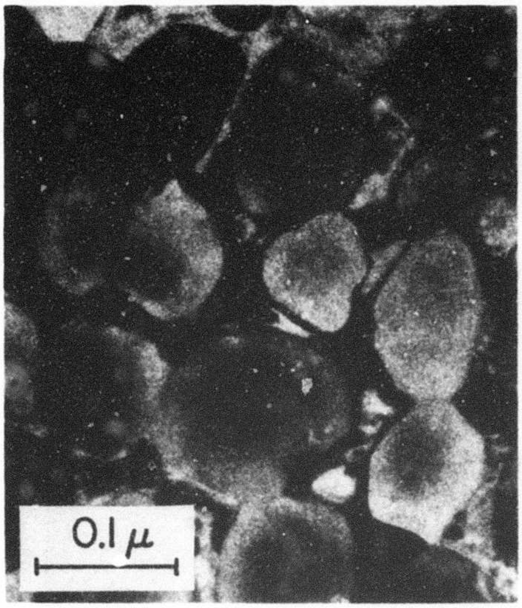

Figure 3c: Bright field micrograph of Fig. 3b Mag: 200,000 x

III. INSTABILITY ASSOCIATED WITH METAL-GLASS INTERACTIONS

In the first semi-annual report, we have reported a study of the interaction between vanadium and thermally-grown SiO_2. The interaction decomposes SiO_2 and results in the formation of a vanadium-rich silicide, V_3Si. It was suggested in the report that the metal-glass interaction may not be unique to V, but is a rather general phenomenon between glass and transition metals that form highly stable oxides. The transition metal oxide which is more stable than SiO_2 provides the driving force for the reactions. In a continuous effort to understanding the glass-metal interaction, we have further investigated the interaction between oxidized silicon and Ti and Nb using a combined technique of x-ray diffraction and ion backscattering. Indeed we found that the results agree very well with our expectation that both Ti and Nb decompose SiO_2 at temperatures above 700°C and 900°C, respectively and form metal-rich silicides, Ti_5Si_3 and Nb_3Si. We note that the Nb_3Si obtained is not a high Tc superconducting phase; it has a F.C.C. structure the same as the ordered Cu_3Au.

Silicide formation in silicon technology is most commonly obtained by a direct reaction between silicon and a vapor deposited metallic film. To compare our glass-metal reaction to silicon-metal reaction from the point of view of silicide formation, we have studied contact reaction between Ti and Si and also Nb and Si. The results again agree with our earlier findings in the case of V and Si; the silicide formed by metal-silicon reaction is silicon-rich $TiSi_2$ and $NbSi_2$.

There exists a distinct difference between metal-silicon and metal-glass reactions from the point of view of silicide formation. As a first step to understanding the cause of the difference, and also because there has recently appeared a large quantity of literature on silicide formation, we have made a review of silicide formation from the viewpoint of their structure, kinetics, and stability. The review is intended to update our understanding of this subject and also to suggest future research directions, in particular, we have pointed out that marker motion in silicides and the effect of a thin oxide on metal-silicon interactions are both crucial areas. Also included in the review is a critical evaluation of sample preparation and experimental techniques of ion backscattering and glancing angle x-ray diffraction as they are applied to study thin film interactions.

A. ANALYSIS OF THIN-FILM STRUCTURES WITH NUCLEAR BACKSCATTERING AND X-RAY DIFFRACTION

J. W Mayer and K. N. Tu

ABSTRACT: Backscattering of MeV ^{4}He ions and Seemann-Bohlin x-ray diffraction techniques have been used to study silicide formation on Si and SiO_2 covered with evaporated metal films. Backscattering techniques provide information on the composition of thin film structures as a function of depth. The glancing angle x-ray technique provides identification of phases and structural information. Examples are given of V on Si and on SiO_2 to illustrate the major features of these analysis techniques. We also give a general review of recent studies of silicide formation.

I INTRODUCTION

The formation of silicide layers has played an important role in integrated circuit technology. Ohmic contacts and barriers on Si are formed by evaporating a metal layer (Pd, Pt, Ti, ...) on Si and subsequently heating to form the metal-silicide.(1) We have utilized backscattering techniques with MeV He ions to study the kinetics of the silicide growth and glancing angle x-ray diffraction techniques to identify the phases that are formed. This paper is a review of the capabilities of these analytical techniques and of the results obtained in our and other laboratories concerning metal-silicon interactions.

The process steps of evaporation and heat treatment are simple and easily adapted to device production. The factors which govern the silicide formation are more complex. Of the twelve metal/silicon systems studied in some detail(2-17), all have between three and seven silicide structures identified in bulk samples(18-21). In thin film structures, typically only one and in a few cases two silicide phases are formed. The lowest eutectic temperatures given in the phase diagrams range between 740°C and 1400°C, yet the silicides form in thin film samples at temperatures between 200° and 800°C. In most cases the formation occurs at temperatures of about one-third to one-half the melting point (in °K). This is a sure sign that solid-solid rather than solid-liquidus reactions are involved. It has recently been found that silicide layers are formed during heat treatment of metal layers on SiO_2(11,16). Usually a different phase is formed and the reaction temperature is 100 to 200°C higher than for the metal/silicon systems.

From an operational standpoint it is of interest to determine the temperatures at which silicide growth occurs, growth rates, identity of the phases, their stability, and the influence of the interface conditions (presence of oxide layer). These aspects are of concern in integrated circuit technology and can be answered directly by the combined use of MeV He backscattering and glancing-angle x-ray diffraction techniques. The underlying problem is to determine what factors govern the nucleation and growth of the silicide. Some insight can be gained by measuring the kinetics of the process and determining which species, Si or metal, diffuses through the silicide layer. Again, backscattering techniques can be used.

II ANALYTICAL TECHNIQUES

A. MeV ^{4}He Ion Backscattering

This technique has been described in detail previously(22-23) and will be discussed only briefly. As shown in Fig. 1, the sample is mounted in a chamber (modest vacuum requirements, $\approx 10^{-5} - 10^{-6}$ Torr) and bombarded with monoenergetic He ions (typically at 2 MeV) at current levels of 20-50 na over about a 2 mm x 2 mm area. Only a small fraction of the incident particles are backscattered so the beam is to first order not attenuated. The silicon surface barrier detector produces a voltage pulse that is proportional to the energy of the individual backscattered He ions. The pulses are amplified and stored in a pulse-height analyzer and at the end of the analysis (generally 15-30 min) the energy spectrum of backscattered particles is displayed.

The energy of particles scattered from surface atoms is determined by the mass of target atom through scattering kinematics K (billiard-ball kinetics), the numer of particles backscattered by the scattering cross-section σ (Rutherford scattering with $\sigma \alpha (Z/E)^2$ in this energy region) and the energy loss in traversing the film by stopping cross section ϵ. All these parameters, K, σ and ϵ, are well known with the major uncertainty in the stopping cross-section ϵ where the values are generally established within ± 5%(24). Consequently, these backscattering spectra give directly and quantitatively the distribution of elements as a function of depth in the target. In effect it provides mass-sensitive depth microscopy.

It should be noted that the depth scale is determined by the number of target atoms/cm^2 in an incremental layer not by the thickness of the layer. Cast in other terms, the density of a thin film can be determined from measurement of the number of target atoms/cm^2 (or from the difference in energy between particles scattered from the front and rear surface of a film) and from an independent measurement of the film thickness by interferometric techniques. For simplicity, the film thicknesses are usually given in dimensions of Å with the assumption of bulk density.

The advantages of backscattering then are: 1) quantitative measurement of composition, 2) non-destructive determination of depth profiles, and 3) simple and direct interpretation of experimental data. The measurements themselves are quite easy to preform.

Some of these features are shown in Fig. 2 which gives backscattering spectra for an evaporated layer of V on Si before and after heat treatment. For the as-deposited case (dashed line), the broad peak is the component of spectrum due to particles backscattered from V. The measured energy difference between particles scattered from the front surface and the back surface of the V layer, i.e. the width of the peak, is 300 keV which corresponds to 2.24×10^{18} V atoms/cm^2 or a thickness of 3100Å if bulk density is assumed. After heat treatment a step appears in both the V and Si portions of the spectrum. This step corresponds to the formation of a silicide layer. The composition can be determined from the ratio of the heights, H, of the V and Si steps, here 1.35, when corrected for the ratio of scattering cross sections, $\sigma_{Si}/\sigma_V = 0.36$. This gives a V/Si ratio of .485 which must be corrected upwards by a factor of 1.04 because of the differences in stopping cross-section for particles scattered from V and from Si. This result shows that in the layer there are two Si atoms for every V atom, an indication that the compound VSi_2 is formed. However, positive identification requires structural data which is provided by x-ray diffraction (see B, below).

The thickness t of the composite layer is determined from the energy width ΔE, here $\Delta E = 140$ keV. Assuming bulk density this gives a thickness of 1700Å. The growth kinetics of the composite layer can be found from the time dependence of ΔE for various heat treatment cycles.

The fact that the edges of the steps are sharp in Fig. 2 demonstrates that the layer is uniform in thickness over the dimensions of the beam. Laterally non-uniformities introduce a broadening in the edges and hence uncertainties in thickness determination. If local cracking or flaking of the film occurs during thermal processing, backscattering spectra are misleading. Hence, one should also examine the lateral uniformity by optical microscopy or preferably by use of a scanning electron microscope.

Backscattering spectra are simple to interpret when there are only a few elements in the target. For multilayer targets, the spectra can be complex. Figure 3 shows spectra for normal incidence and 45° beam to target orientation for a twelve layer ThF_4-ZnS reflective coating. The distinct peaks reflect the Th in the twelve ThF_4 layers and the valleys show the position and thickness of the ZnS layers. The contribution from the Zn, S, and F can not directly be seen in the spectra. The arrows indicate their energy position if located at the surface. The two peaks at the highest energy are flat topped and have sharp edges indicated well defined layers of uniform composition. At lower energies (greater depths in the multilayer structure) the broadening of the edges reflect both a loss of depth resolution due to energy straggling and interference from lower mass elements.

B. Seemann-Bohlin X-ray Diffraction

The Seemann-Bohlin configuration for structural analysis of thin films is basically a glancing angle x-ray diffraction using a focused beam with a fixed angle of incidence. It is known that to study the structure of a polycrystalline thin film of thickness of the order of 10^2 to 10^4 Å is difficult by conventional x-ray techniques because there is not much material for scattering. However, scattered beams can be strengthened by increasing the path of x-ray in the film by the use of a fixed incident beam at a near-grazing incidence, and we note that such a fixed incident beam can be obtained in a diffractometer based on the focusing Seemann-Bohlin configuration but not on the conventional Bragg-Brentano configuration(25). In the focusing

Seemann-Bohlin configuration, see Fig. 4, the specimen is placed on the circumference of the diffraction circle and the angle of incidence is fixed and can be made as small as a few degrees, for example, an incident angle of 6.4° in this case will increase the length of the path of the beam in the specimen to about 9 times its thickness. The specimen, the focus "F" of the monochromatic incident beam and the focus of the diffracted beams all lie ideally on the circumference of the diffraction circle. Based on this principle, Feder and Berry(26) have designed and built a x-ray diffractometer with a diffraction circle of 20 inches in diameter. An important feature of the diffractometer is that it employs a pyrolytic graphite monochromator crystal to produce a high intensity monochromatic Cukα radiation as the incident beam. The intensity obtained from the graphite crystal is 15 times greater than that obtained from a LiF crystal. Also a circular helium chamber of 18 inches in diameter is interposed in the path of the diffracted beams to reduce the atmospheric absorption.

The performance of the diffractometer has been discussed elsewhere(26). We mention briefly here that it has detected a polycrystalline copper film of 150Å and showed a precision lattice parameter measurement of a number of 1000Å nickel films with an accuracy of ± 0.0001Å, i.e. 1 part in 35000. In addition to the high sensitivity of detecting phases, the Seemann-Bohlin diffraction allows convenient structural analysis of grain size, biaxial strain and the distribution of pole densities. This is because its reciprocal lattice vector "$\vec{H}$" of Bragg diffractions are not parallel to the normal "n" of the film surface but rather make inclination angles with the normal. The angle increases with the order of the reflections. Thus each reflection measures in a different direction the lattice parameters, the size and the total amount of coherently diffracted regions. It is clear that this type of diffractometer can deliver a great deal of structural information of polycrystalline thin films. We should note that single crystal films are not suitable for Seemann-Bohlin diffractometer and the diffraction patterns may show no peaks at all. This may be regarded as advantageous for a polycrystalline film on a single crystal substrate such as a metal film on a Si wafer since we do not need to worry about the interference of Si reflections.

It seems that for a structural study of thin films of thickness around 1000Å and less, we can use transmission electron microscope, for films thicker than several microns we can use conventional x-ray equipment, and for films in between, we use Seemann-Bohlin type x-ray diffractometer.

The diffractometer is expected to be very powerful in the investigation of the interaction in thin films(27), because the reaction products can be identified by their x-ray reflections very early in the diffusion cycle. Figure 4 shows the x-ray pattern of a sample of 3200Å of vanadium on a Si wafer that has been heat treated at 800°C for 15 minutes. The pattern was obtained by scanning the sample with CuKα radiation at steps of 0.15° (4θ) increment and with a counting time of 30 seconds at each step. The peaks have been indexed as reflections of VSi_2 according to ASTM card #13-260. In this sample, the x-ray diffraction data confirm the composition analysis determined from backscattering data (Fig. 2).

III ANALYSIS OF SILICIDE FORMATION

A. General Precautions

One of the objectives of this type of analysis is to determine the growth kinetics. It is a course fraught with peril and sample preparation is the dominant factor. There are three areas which must be considered: interface, contamination, and stress.

1. Interface. The native oxide layer on silicon surfaces must be considered when preparing samples. It has been shown that thin oxide layers significantly retard silicide formation.(6) The thickness of native oxide layer is markedly different for different wafer orientations(28) and hence sample orientation plays a role. Soaking in HF and then rinsing prior to mounting in the evaporation chamber does not guarantee an oxide free surface. One approach is to sputter clean the surface and then deposit the metal layer without breaking vacuum. Although this creates reproducible surface conditions, the silicon surface is heavily damaged and the sputtering gas is retained in the surface layer.(29)

2. Contamination. Oxygen and other ambient contaminations can be introduced during deposition or thermal processing. Trace inclusions of oxygen are hard to detect by backscattering techniques, although relatively massive concentrations (10 to 20 at.%) can be readily identified. There has not been a positive correlation of film contamination with retardation of silicide growth; however, preliminary data suggest that this may be a real problem.(30)

3. Stress. One of the most difficult factors to overcome is film cracking or peeling due to stress created during thermal processing.

Backscattering measurements on such samples are unreliable. Film peeling is often enhanced for thicknesses greater than a few thousand Angstroms. In some cases, this problem can be alleviated by maintaining an oxide free interface or depositing the film at elevated temperatures.

There is of course the polycrystalline nature of the deposited and reacted film that should be considered. Grain size and grain boundary diffusion may be important particularly at low process temperatures ($T \lesssim 400°C$). These problems have not been properly addressed in silicide formation, but are known to occur in metal-metal thin film studies. At higher temperatures bulk diffusion will probably dominate over grain boundary effects.

B. An Example: V-Si System

Backscattering analysis have been applied to nearly a dozen silicide systems. Two of which (Pd-Si(3,6,9,10,12-14) and Hf-Si(7,8)) have been studied in detail. We have chosen the vanadium silicide system as an example because the problems are still fresh (as the study has not been completed) and also we can consider aspects of silicide formation on SiO_2. Our work(11,16) with Ti, Nb and V deposited on SiO_2 shows that silicides are formed but at higher processes temperature than for Si/metal systems and that the silicide is metal rich.

Figure 6 shows backscattering spectra for V films deposited on SiO_2(30). For the as-deposited case (dashed line in Fig. 6B) the spectrum shows the contribution from V, Si in the oxide layer and substrate, and oxygen in the oxide layer. The oxygen contribution is superimposed on that from the underlying Si substrate. The arrows indicate the energy position of these elements when at the surface. Following heat treatment in oxygen at 400°C there is a change in the composition of the sample. Oxygen is now present at the outermost layers (I) as evident in Fig. 6A from the step in the V component and the appearance of a broad mesa whose high energy edge corresponds to the position of oxygen at the surface. There is not a significant amount of oxygen in underlying V layer (II) as indicated by i) the height of the V portion of the spectrum (layer II) coincides with the as-deposited case and ii) there is a dip in the oxygen component of the spectrum in the region between that from oxygen in SiO_2 (III) and in Vandium oxide (I).

The composition of the Vandium oxide can be estimated from ratio of the heights of Vandium and oxygen components in region I to be close to that of V_2O_5. Positive identification was made from glancing angle x-ray diffraction data (Fig. 7). The peaks correspond to those indexed for V_2O_5.

Referring again to Fig. 6, it is evident that there is a dramatic change in composition when a similar sample is heated to 800°C in vacuum. The composition of the layers can be deduced from the spectrum to show:

Layer I: Approximately equal amounts of Vandium and oxygen with no appreciable concentration of Si.

Layer II: Three times as much V as Si and no appreciable oxygen.

Layer III: SiO_2 but of reduced thickness. The amount of oxygen removed from the initial thickness of SiO_2 (III) corresponds to the amount added to the vanadium oxide layer (I) indicating that the amount of oxygen in the composite layers is conserved.

The x-ray diffraction data for this sample coincides with that given by Tu et al(11) for a similar sample and shows the presence of V_3Si, V_5Si_3 and V_2O_5. The major feature is the predominance of V_3Si for this sample whereas VSi_2 is formed in the V/Si samples.

There are two unusual features in this comparison between backscattering and x-ray diffraction data. Backscattering data indicate a 1:1 ratio of V to O and diffraction data indicate V_2O_5. This may be due to the fact that the V_2O_5 eutectic is at a lower temperature(18) than the 800°C process temperature. We suggest that oxygen dissolves in the vanadium at the process temperature and then the V_2O_5 nucleates as crystallites imbedded in a matrix of vanadium when the sample cools below the eutectic. However, the average V/O ratio over the entire vanadium-oxide film thickness could be near unity as indicated by backscattering data. The other question concerns the location of the V_5Si_3 identified in x-ray diffraction. Backscattering data(16) do not show appreciable amounts of Si near the surface (region I in Fig. 6B) and the spectrum height ratio for the silicide layer (region II) corresponds to V_3Si. At present we suggest the V_5Si_3 is located near the interface between region I and II.

This example clearly shows the drastic effect that a thin oxide can have on both growth kinetics and silicide composition. In this case, the metal-rich silicide is of interest in its own right as a superconductor with a transition temperature of 17°K(11).

IV SILICIDE FORMATION

In this section we will review experimental data on silicide formation from the standpoint of structure, thermodynamics and kinetics. We also include some speculations and suggestions for future work. Figure 8 gives a general impression of results obtained and more details are given in Table I.

A. Structure

The typical silicide which is formed with metal/Si interaction is the phase which is most rich in Si, i.e. PtSi and $CrSi_2$. This is the end point which one expects from an equilibrium point of view. There should be two phases, Si and the most Si rich silicide. It is surprising that more phases do not appear as one would expect all phases to be present during the reaction stage. Indeed intermediate phases (Pd_2Si, Pt_2Si, HfSi and NiSi) have been detected in a few systems. Other phases may be present but their extent is determined from kinetic considerations of diffusion rate and nucleation. Kidson[32] had earlier pointed out that if the rate constants of diffusion in a given phase are small the phase layer may be too thin to be detected.

The microstructure of HfSi, $HfSi_2$, VSi_2, PtSi and Pd_2Si has been measured by x-ray diffraction. As a first approximation the grain size of the silicide is about the same as the deposited metallic film ($\sim$ 200-500Å). There have not been serious attempts to measure strain in the silicide layer and its dependence on heat treatment temperature. This is clearly one area that should be explored further.

Even though the crystal structure of most silicides are different from Si, they tend to show some preferred orientation. The most striking case is Pd_2Si which has been shown by both reflection-electron diffraction and MeV $^4He^+$ channeling techniques to grow epitaxially on <111> Si.[10,12-14] In this case the hexagonal basal plane of Pd_2Si matches quite well with the <111> Si structure. Similar considerations of lattice matching suggest that $NiSi_2$, $CoSi_2$ and $FeSi_2$ may also form epitaxially. This conclusion has not been tested and is an obvious area for further study.

B. Thermodynamics

Silicide formation energies have been tabulated[33] for the following four systems: Mo/Si, Ta/Si, Ti/Si, and Zr/Si. In the Mo/Si system, $MoSi_2$ is the most stable phase among the Mo-silicides and was found to be the predominant phase in backscattering measurements. $TaSi_2$ is equally stable as compared to the Ta-silicides; however there have been no measurements of silicide formation in evaporated Ta films on Si. For the Ti/Si and Zr/Si systems the monosilicides, TiSi and ZrSi, have lower free energies than the disilicides $TiSi_2$ and $ZrSi_2$. This suggests that before the formation of the disilicide an intermediate stage might be observed. There is no direct evidence for this although our preliminary results[33] on Ti/Si hint at the presence of an intermediate phase before $TiSi_2$ is formed. In the Hf/Si system, which should be analogous to Zr/Si, HfSi does form and is stable up to temperatures of $\approx$ 750°C where $HfSi_2$ forms. In spite of these indications we believe that there is not yet sufficient evidence to make a strong correlation with formation energy. This situation might be improved if measurements were made on the Ta/Si system and further measurements were carried out in the Mo/Si system.

From a conventional standpoint, the stability of a phase is indicated by its melting point. This may be misleading and should not be used as a guide to predict which forms first. It is interesting to note, however, from Table I that a value of half the melting point in °K is rough guide to the minimum temperature at which silicide formation has been observed. This may be too high an estimate because HfSi, Pd_2Si, WSi_2 and PtSi form at about one-third the melting point. In fact the one-third relation may be the rule rather than the exception because oxide layers at the interface will raise the formation temperature. For example, the published NiSi formation temperature of 600°C is higher than that of 300°C recently obtained in a separate investigation[34]. We suspect that the presence of the native oxide layer on Si might be responsible for the high temperature found for the Mo/Si system.

We can consider other aspects such as epitaxial growth that might effect stability. Hutchins and Shepala[12] showed for transformation of Pd_2Si to PdSi that higher temperatures are required on <111> oriented Si than on <100>. On <111> oriented Si, Pd_2Si shows the strongest orientation. While Pd_2Si is very stable (200°C-700°C), Pt_2Si is not and transforms to PtSi quite easily. One reason might be that Pd_2Si is epitaxial and has a higher melting point than PdSi while Pt_2Si does not show good epitaxy and has a lower melting point than PtSi.

For Pt_2Si one finds the low-temperature, (tetragonal) phase in these silicides rather than the high temperature (hexagonal) phase; the polymorphic transition temperature is at about 700°C. We attempted to form this hexagonal phase (which should epitaxial on <111> Si) by heating a sample to 750°C for 30 min. Backscattering data[34] showed that PtSi (3% Si rich) rather than Pt_2Si was formed. Consequently this attempt to form a more stable phase of Pt_2Si was not successful.

C. Kinetics

From the standpoint of kinetics, the important factors are the mechanisms for transporting metal or Si across the silicide layer, the activation energy and the identity of the diffusing species. Most silicides tend to react at temperatures above 500-600°C except for the Pd/Si and Pt/Si systems which react at temperatures as low as 200°C. The activation energy measured for the growth process for these latter silicides is between 1.1 and 1.5 eV. This is remarkably low and opens the question of grain boundary growth. We believe however that bulk diffusion dominates. The structure of Pd_2Si is very open and interdiffusion is expected to be fast. Further the same activation energy was found from 100° to 700°C indicating that the same diffusion mechanism was involved. Also the same growth rate is found for Pd_2Si on different oriented Si samples where the amount of epitaxy is different. In cases where there is less epitaxy, one anticipates more large-angle grain boundaries and increased grain boundary diffusion. All these findings support the dominance of bulk diffusion even at temperatures of 200°C.

The other silicides react at higher temperatures and we would expect lattice diffusion to be dominant. The activation energy for diffusion has only been measured in a few cases but seems to be above 2 eV (2.5 eV for HfSi, 2.9 for VSi_2 and 2.7 for WSi_2). These values are too high for grain boundary diffusion and suggest bulk effects. One would expect to see grain boundary diffusion at lower temperatures. This could be tested by prolonged heating of a sample at temperatures below the reaction temperatures and looking for Si accumulation at the free surface. This interface accumulation is often seen in backscattering studies of metal-metal interactions at low temperatures. However, no systematic studies have been made on metal/Si systems.

The growth of most silicides (HfSi, Pd_2Si, Pt_2Si, PtSi, $TiSi_2$, WSi_2 and VSi_2) have been found to follow an $(time)^{1/2}$ relationship characteristic of a diffusion dominated process. In two cases, $CrSi_2$ and $MoSi_2$ a linear growth has been found.[6] These systems have not been studied in detail and we cannot speculate on the reasons for the linear growth rate. In fact, the growth kinetics of all the high temperature silicides has not been followed in as much detail as has been done for Pd/Si and Pt/Si. There is a need for careful kinetic studies on samples with oxide free interfaces between metal and Si.

There is one other notable gap in all the data. With the exception of HfSi, there is no evidence to indicate whether Si or metal is the diffusing species through the silicide layer. This data could be obtained by implanting rare gas atoms into the silicide and using backscattering techniques to determine whether the gas atoms moves toward or away from the surface. Similar studies have been made with anodic oxidation.[35] For the Hf/Si system, the argon that was present as an impurity introduced during deposition served as a marker.[7] The data indicated the Si was the diffusing species. There are practical implications. If Si is the diffusing species, it will leave vacancies near the Si/silicide interface. If these vacancies condense into voids, it leads to easy peeling of the silicide under stress.

D. Comparison with M/SiO_2 Reactions

It has recently been found the silicide formation can occur with metals in contact with SiO_2.[11,16] The behavior of V/SiO_2 and V/Si has been discussed above in Sec. IIB. In the case of Ti, Nb, and V the silicide was the more metal rich phase.[16] At present our work is in too early a stage to give any insight into this behavior. One immediate question is to determine if the Si rich phase forms when the SiO_2 layer is consumed.

V SUMMARY

This review was intended as a survey of metal-silicide formation studies where both backscattering and x-ray diffraction measurements have been utilized. These techniques complement each other as backscattering data gives composition as a function of depth and hence can be used to determine growth kinetics while x-ray diffraction gives identification of phases and structural information.

A survey of silicide formation for metal films deposited on Si indicates that the typical silicide that is formed is the phase that is most rich in Si. This is the end point one expects from thermodynamic equilibrium considerations. In some cases intermediate phases; have been found. On the basis of present data we have not been able to find general guidelines that can be used to predict when such an intermediate phase will occur. One striking observation is that metal rich silicides are formed when the metal layer is deposited on SiO_2 rather than on Si.

The formation temperature on the silicides is generally between one-third to one-half the silicide melting point in °K. This shows that solid-solid rather than solid-liquidus reactions are involved. The growth kinetics of the silicide with two exceptions have been found to follow a $(\text{time})^{1/2}$ dependence typical of diffusion limited reactions. We believe that bulk rather than grain boundary diffusion is involved. There have not been studies to determine whether the metal or the Si is the diffusing species except for the Hf/Si case where Si appeared to migrate.

Our survey indicates that only the most general features of silicide formation have been studied. There are a number of areas that require further investigation. Until these are carried out it is difficult to present an overall picture of the factors which control silicide formation.

ACKNOWLEDGMENT

The authors acknowledge with pleasure discussions with our colleagues: C. J. Kircher and J. F. Ziegler at IBM; M-A. Nicolet, W-K. Chu, and H. Kraütle at Caltech. We thank H. Kraütle for his data on V/Si and V/SiO_2.

REFERENCES

1. M. P. Lepselter and J. M. Andrews, in Ohmic Contacts to Semiconductors, edited by B. Schwartz (The Electrochemical Society, New York, 1969) p. 159.
2. M. P. Lepselter and S. M. Sze, Bell Syst. Tech. J. 47, 89 (1969).
3. C. J. Kircher, Solid State Electr. 14, 507 (1971).
4. A. Hiraki, M-A. Nicolet and J. W. Mayer, Appl. Phys. Lett. 18, 178 (1971).
5. H. Muta and D. Shinoda, J. Appl. Phys. 43, 2913 (1972).
6. R. W. Bower and J. W. Mayer, Appl. Phys. Lett. 20, 359 (1972).
7. C. J. Kircher, J. W. Mayer, K. N. Tu and J. F. Ziegler, Appl. Phys. Lett. 22, 81 (1973).
8. J. F. Ziegler, J. W. Mayer, C. J. Kircher and K. N. Tu, J. Appl. Phys. (Sept. 1973).
9. R. W. Bower, R. E. Scott and D. Sigurd, Solid State Electr. (to be publ.).
10. D. Sigurd, W. Van der Weg, R. Bower, and J. W. Mayer, Conference on Ion Beam Analysis of Surface Layers, 1973, Thin Solid Films (to be publ.).
11. K. N. Tu, J. F. Ziegler, and C. J. Kircher, Appl. Phys. Lett. (to be publ.).
12. G. A. Hutchins and A. Shepala, Thin Solid Films (to be publ.).
13. D. H. Lee, R. R. Hart, D. A. Kiemet, O. J. Marsh, Phys. Stat. Sol.(a) 15, 645 (1973).
14. W. D. Buckley and S. C. Moss, Solid State Electr. 15, 1331 (1972).
15. K. E. Sundström, S. Petersson, P.-A. Tove, Uppsala University Report, UPTEC 73-29R (to be publ.).
16. H. Kraütle, M-A. Nicolet, and J. W. Mayer, Phys. Stat. Sol.(a) (to be publ.).
17. J. A. Borders and J. N. Sweet, Sandia Laboratories, private communication.
18. M. Hansen, "Constitution of Binary Alloys" (McGraw-Hill, New York, 1958).
19. R. P. Elliott "Constitution of Binary Alloys, First Supplement" (McGraw-Hill, New York 1965)

20. F. A. Shunk, "Constitution of Binary Alloys, Second Supplement" (McGraw-Hill, New York, 1969).

21. W. B. Pearson "Handbook of Metals and Alloys" (Pergamon Press, Oxford, 1967) Vol. 2.

22. M-A. Nicolet, J. W. Mayer, and I. V. Mitchell, Science 177, 841 (1972).

23. W. K. Chu, J. W. Mayer, M-A. Nicolet, T. M. Buck, G. Amsel, and F. H. Eisen, Thin Solid Films 17, 1 (1973).

24. W. K. Chu, J. F. Ziegler, I. V. Mitchell and W. D. Mackintosh, Appl. Phys. Lett. (to be publ.).

25. B. D. Cullity, "Elements of x-ray Diffraction" (Addison-Wesley, Reading, Mass., 1956).

26. R. Feder and B. S. Berry, J. Appl. Cryst. 3, 372 (1970).

27. K. N. Tu and B. S. Berry, J. Appl. Phys. 43, 3283 (1972).

28. W. K. Chu, E. Lugujjo, J. W. Mayer and T. Sigmon, Conference on Ion Beam Analysis of Surface Layers, 1973 (to be publ. in Thin Solid Films).

29. G. W. Sachse, W. E. Miller, and C. Gross, submitted to Solid State Electronics.

30. H. Kraütle, Caltech (private communication).

31. C. J. Kircher, J. F. Ziegler, IBM (private communication).

32. G. V. Kidson, J. Nuclear Materials, 3, 21 (1961).

33. R. Hultgren, R. L. Orr and K. Kelley, "Supplement to Selected Values of Thermodynamic Properties of Metals and Alloys" issued in loose-leaf form by Dept. of Minearl Technology, University of California, Berkeley, Calif.

34. K. N. Tu and W. K. Chu (unpublished data).

35. F. Brown and W. D. MacKintosh, J. Electrochem. Soc. (to be published).

Table I SILICIDE FORMATION

Metal+	Phases	Structure	Backscattering Phase	 T_{obs} °C	 Kinetics	T_{melt} °C	$\frac{T_{obs}\ °K}{T_{melt}\ °K}$	Ref
Ti (3)	Ti_5Si_3	hexagonal	--			2120		
	TiSi	orthohombic	--			1700		
	$TiSi_2$	" (C49)	$TiSi_2$	600	$t^{1/2}$	1540	≈0.5	6
Zr (7)	Zr_2Si	tetragonal	--			2110		
	ZrSi	ortho	--			2095		
	$ZrSi_2$	" (C49)	$ZrSi_2$	700	--	1520	≈0.5	15
Hf (5)	Hf_2Si	tetra				2430		
	HfSi	ortho or hexa (FeB)	HfSi	550	$t^{1/2}$	2200	≈0.3	
	$HfSi_2$	ortho (C49)	$HfSi_2$	750		1900	≈0.5	7,8
V (3)	V_3Si	cubic (β-W)				2070		
	V_5Si_3	tetra (D8m)				2150		
	VSi_2	hexa (C40)	VSi_2	600	$t^{1/2}$	1750	≈0.5	11,16
Nb (4)	Nb_4Si	hexa						
	Nb_3Si	cubic (Cu_3Au)						
	$NbSi_2$	hexa (C40)	$NbSi_2$	650			≈0.5	30
Ta (3)	Ta_2Si	tetra (Al_2Cu)				2460		
	$TaSi_2$	hexa (C40)				2200		
Cr (5)	Cr_3Si	cubic (β-W)				1730		
	CrSi	cubic (FeSi)				1600		
	$CrSi_2$	hexa (C40)	$CrSi_2$	450	t	1550	≈0.4	6,15
Mo (3)	Mo_3Si	cubic (β-W)				2120		
	$MoSi_2$	tetra (C11b)	$MoSi_2$	1200	t	2050	≈0.6	6
W (2)	W_3Si_2	tetra				2350		
	WSi_2	tetra (C11)	WSi_2	650	$t^{1/2}$	2165	≈0.35	17
Ni (6)	Ni_3Si	cubic (Cu_3Au)				1165		
	NiSi	ortho (MnP)	NiSi	600		992	≈0.7	
	$NiSi_2$	cubic (CaF_2	$NiSi_2$	800		993	≈0.85	15
Pd (3)	Pd_3Si	ortho (Fe_3C)				960		
	Pd_2Si	hexa (Fe_2P)	Pd_2Si	200	$t^{1/2}$	1330	≈0.35	3,6,9,10 12,13,14
	PdSi	ortho (MnP)	PdSi	735		1090	≈0.75	14
Pt (5)	Pt_3Si	mono				870		
	Pt_2Si	hexa (Fe_2P) tetra (Al_2Cu)	Pt_2Si	200	$t^{1/2}$	1100	≈0.4	
	PtSi	ortho (MnP)	PtSi	200	$t^{1/2}$	1229	≈0.35	4,5

+The number in parentheses indicated the number of phases found in bulk samples.(18-20)

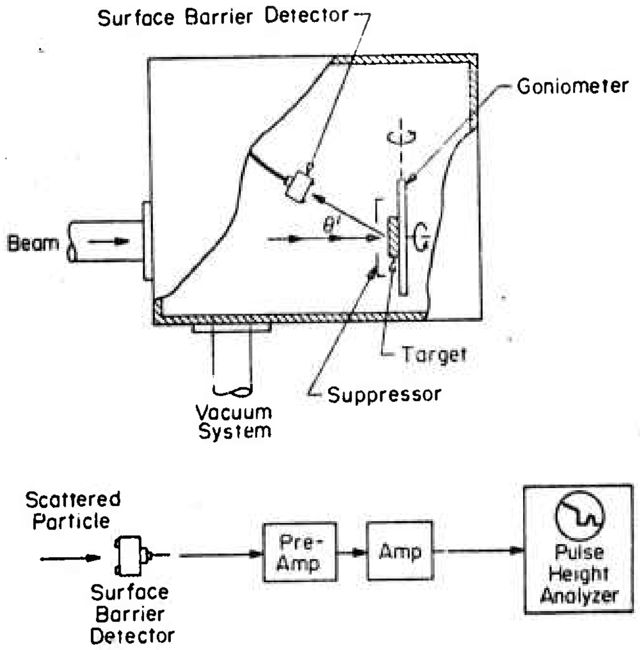

Figure 1. Schematic diagram of the sample chamber used in backscattering measurements.

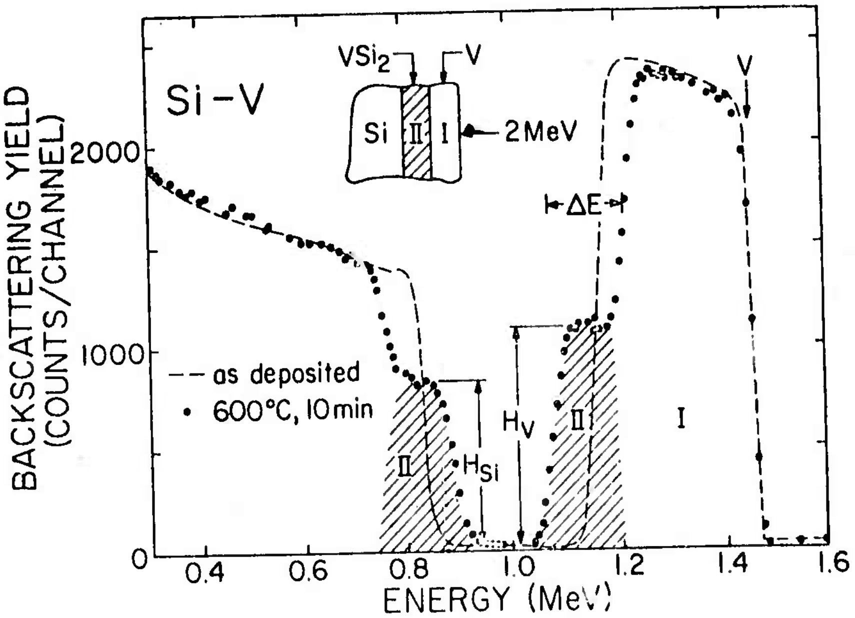

Figure 2. Backscattering spectra for 2 MeV ^{4}He ions incident on Si sample covered with 3100Å of V and heat treated at 600°C. Data from H. Kraütle$^{(16)}$.

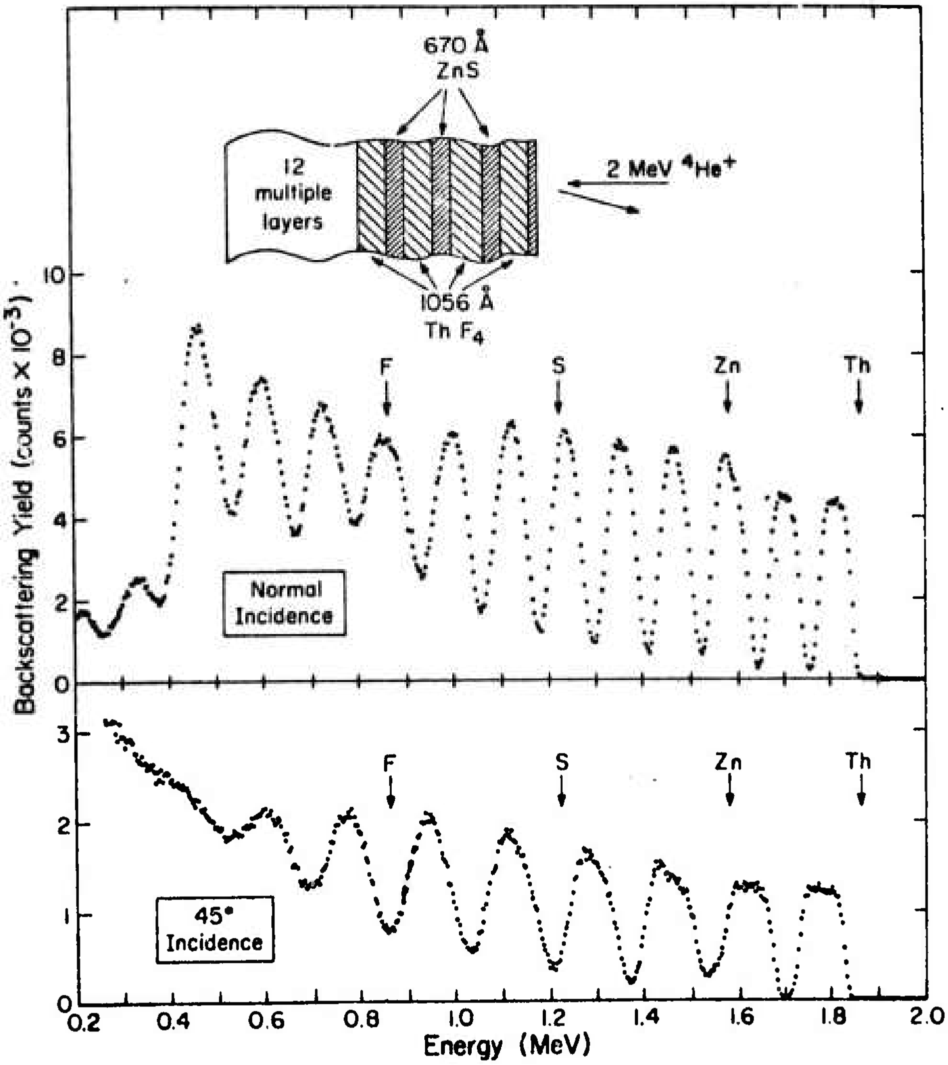

Figure 3. Backscattering spectra for 2 MeV ^{4}He ions incident on a multilayer antireflecting coating on quartz substrate. There are 12 layers of ThF_4 separated by layers of ZnS (sample supplied by R. Honig, RCA).

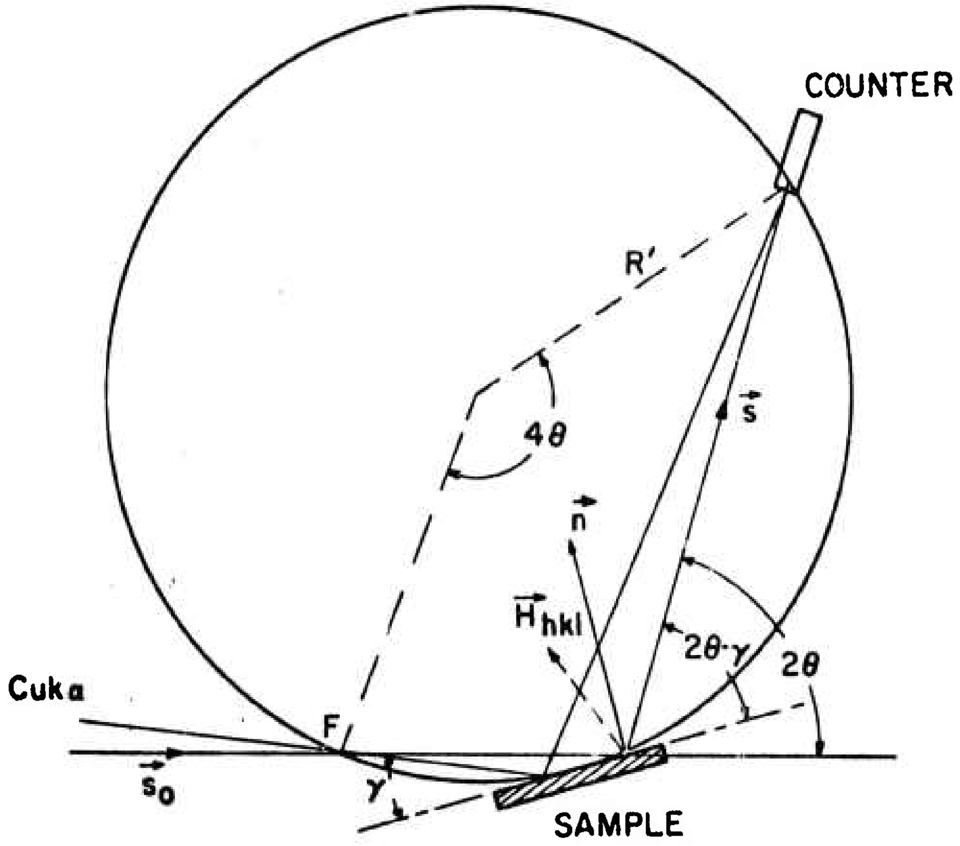

Figure 4. Schematic diagram of the geometry of Seemann-Bohlin diffraction configuration.

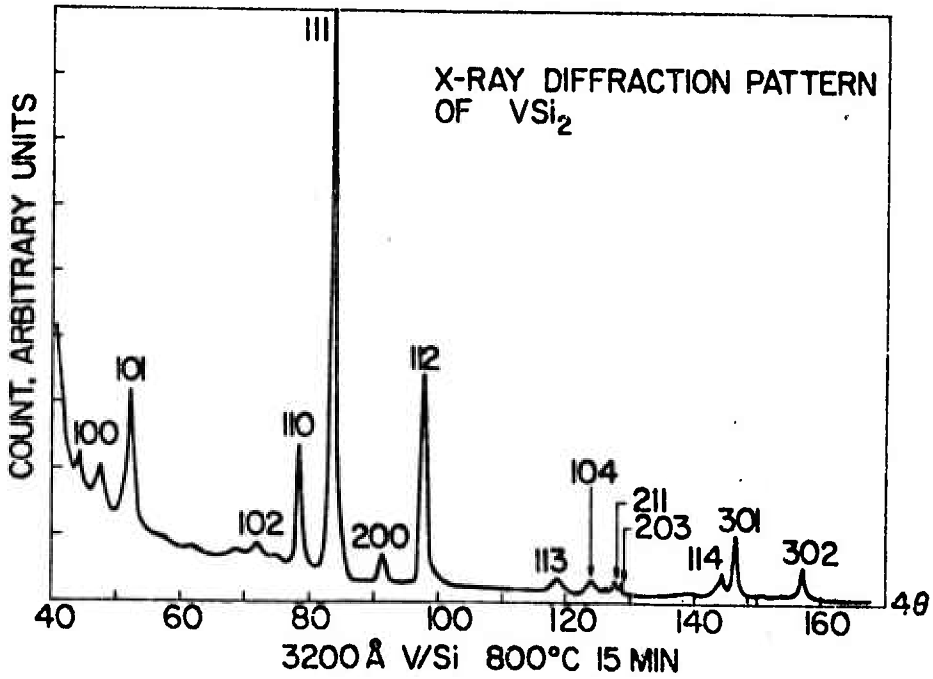

Figure 5. X-ray diffraction pattern of V/Si heat treated at 800°C for 13 minutes in an oxygen free furnace. The vanadium film had a thickness of 3200Å. Reflection of VSi_2 are indexed.

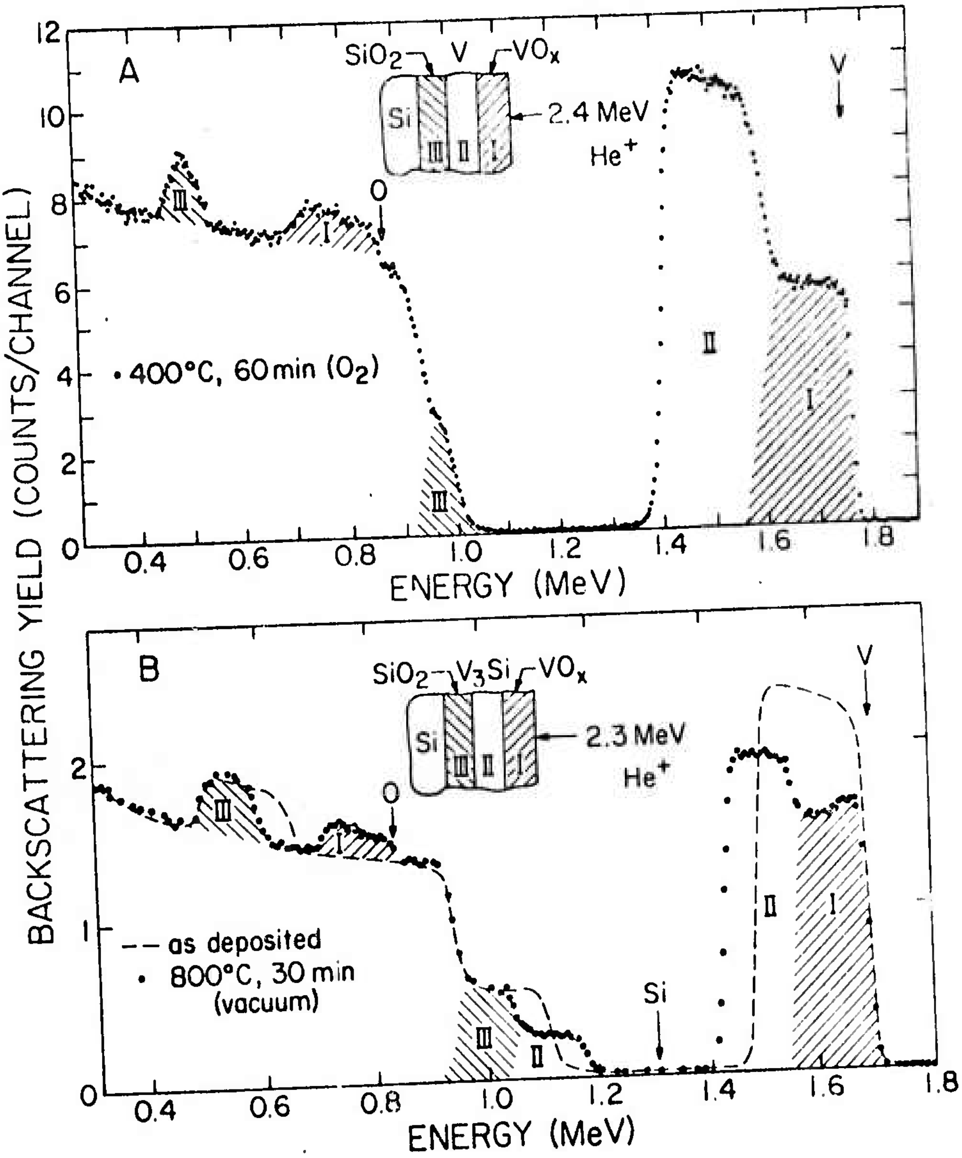

Figure 6. Backscattering spectra for 2.3 MeV ^{4}He ions incident on a Si sample with a thermally grown layer of SiO_2 covered with an evaporated layer of V. A) heat treatment at 400°C for 60 min. in O_2 ambient, and B) heat treatment at 800°C for 30 min. in vacuum. Data from H. Kraütle(16).

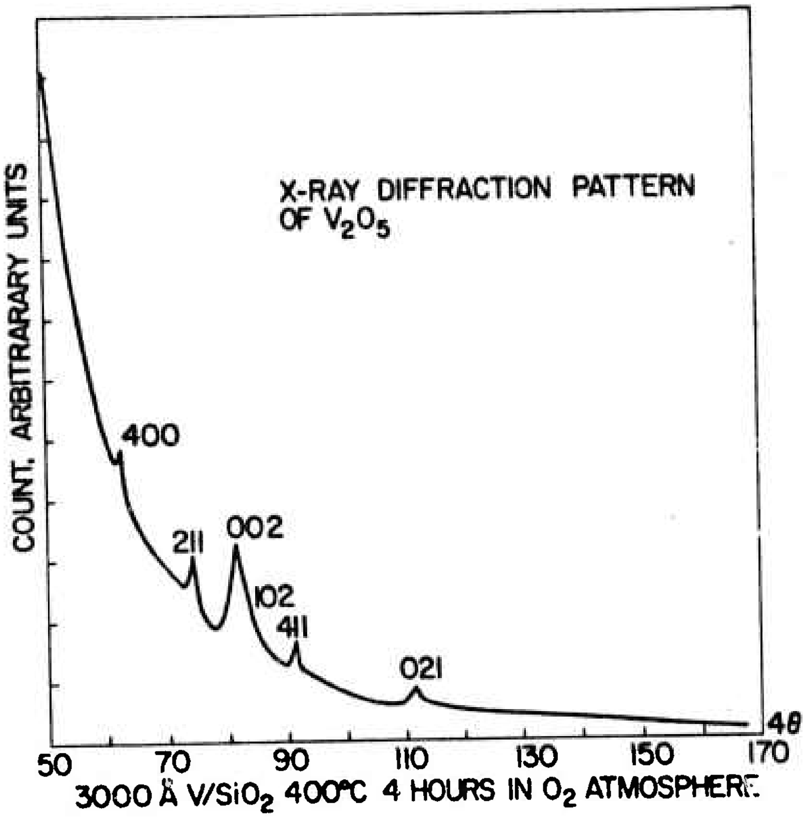

Figure 7. X-ray diffraction pattern of V/SiO_2 heat treated at 400°C for 4 hours in an atmosphere of O_2 + H_2O. The vanadium film had a thickness of 3000Å. Reflection of V_2O_5 are indexed.

SILICIDE FORMATION

IVB	VB	VIB	VIII
Ti *	V	Cr	Ni
$TiSi_2$ (600°)	VSi_2 (600°)	$CrSi_2$ (450°)	NiSi (600) $NiSi_2$ (800°)
Zr	Nb	Mo	Pd*
$ZrSi_2$ (700)	$NbSi_2$ (650)	$MoSi_2$ (1200?)	Pd_2Si (200) PdSi (740°)
Hf *	Ta	W	Pt*
HfSi (550) $HfSi_2$ (750)		WSi_2 (650°)	Pt_2Si (200°) PtSi (300°)

Figure 8. A comparison of silicide formation in thin metal films deposited on Si. The numbers in parentheses indicate the temperature at which silicide formation was observed by backscattering techniques. The asterixes indicate silicides that have been identified by diffraction techniques.

B. REACTIONS OF THIN METAL FILMS WITH Si OR SiO_2 SUBSTRATES

H. Kräutle, W. K. Chu, M-A. Nicolet, J. W. Mayer
California Institute of Technology
Pasadena, California 91109

and

K. N. Tu
IBM Thomas J. Watson Research Center
Yorktown Heights, New York 10598

ABSTRACT

The changes in vacuum-evaporated films of Ti, V and Nb on Si and SiO_2 substrates after thermal anneals are investigated by backscattering and by x-ray spectrometry. Backscattering analysis provides the relative atomic composition as a function of depth with high sensitivity. Glancing x-ray spectrometry detects the chemical composition with high specificity. Combined, the two methods create a specific picture of the transformations induced in the films by the thermal treatment. Generally the reaction on a pure Si substrate produces a Si-rich silicide and on a SiO_2 a metal rich silicide layer as an intermediate layer largely free of oxygen. The oxygen originally bound to the Si in the SiO_2 is transferred to the remaining metal layer. Residual oxygen in the metal film and metal oxides on the metal film influence the silicide formation.

I. INTRODUCTION

Transition metals, and Ti in particular, are used extensively in metallization schemes for integrated circuits and solar cells. Good adhesion and uniformity of the resulting contact are main reasons for their frequent application. The latter aspect has recently been investigated in connection with the Al-Ti metallization scheme.(1) The possibility to form superconducting silicides of transition metals by thin film reactions with the substrate has prompted Tu, et al. to investigate the behavior of V on Si and SiO_2 substrates.(2) The strong affinity of Ti and V for oxygen is believed to be the reason why these metals make good blocking contacts to p-type semiconductor oxides and good ohmic contacts to n-type oxides.(3) Niobium (Columbium) maintains high mechanical strengths at elevated temperatures, but oxidizes readily unless protected by a coating. The disilicide constitutes such a protective layer, based on the ability of the coating to generate a silica[illegible]ed glassy oxide as protection against the atmosphere.(4)

Preliminary data indicate that the heat treatment of these metal films on Si results in the formation of silicides, but that the same metal films deposited on SiO_2 forms both silicides and oxides, generally separated in distinct layers.(5) We present here a systematic study of samples annealed in both vacuum and in dry oxygen. Comparative investigations such as these should lead to insight in the dominant processes at work in these thin films, and to a better understanding of their applications.

II. METHODS AND ANALYSES

A. Backscattering Spectrometry

In this study, the depth and mass perception of backscattering analysis are used to determine the relative atomic composition of the films. The backscattering technique and the brief, a monoenergetic and well collimated beam of $^4He^+$ ions with energy ranging from 2.0 to 2.4 MeV impinges perpendicularly onto the sample. A small fraction of these ions is scattered back into a surface barrier Si detector which is mounted at an angle of 168 degrees against the incident beam. The detector signals are amplified, shaped, and recorded in a multi-channel analyzer. The resulting energy spectrum (counts per energy interval versus energy) furnishes the information of atomic composition versus depth.

As an example, Fig. 1a shows an energy spectrum of 2 MeV $^4He^+$ backscattered from 2100Å of vandium deposited on 2700Å of thermally grown SiO_2 on a Si substrate. Helium ions backscattered from oxygen, silicon and vanadium atoms in the sample have energies which depend on the mass of the scattering atom and its location in depth. After the same sample is annealed in vacuum at 800°C for two hours, the backscattering analysis is repeated and the energy spectrum given in Fig. 1b is obtained. For ease of interpretation, various areas under the energy spectra which correspond to different layers have been shaded (see also insert in the figures). The two spectra clearly differ, as can be seen in Fig. 1b where for comparison the spectrum of Fig. 1a is replotted as a dashed line. The formation of two distinct layers (V_3Si and VO_x) and the remaining part of the SiO_2 is readily distinguished.

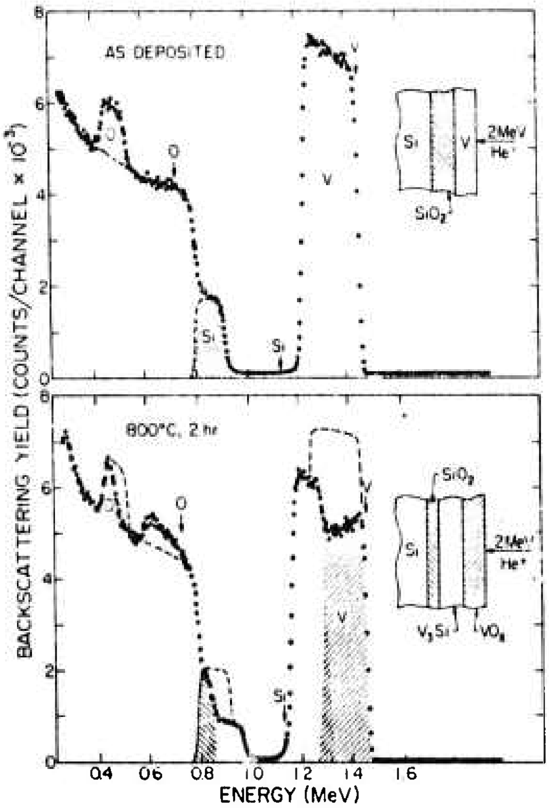

Figure 1. Spectrum of 2 MeV He$^+$ backscattered from a V film on an SiO$_2$ layer on Si as evaporated (top), and after heat treatment in vacuum at 800°C for 2 hours (bottom).

One can convert a backscattering energy spectrum into an atomic concentration profile with the energy loss factor [S] = ΔE/Δx which relates a change in ΔE in backscattering energy to a change Δx in the depth of the sample.(6) The [S]-factor depends, among others, on the energy of the incident particle and the composition of the layer. The energy dependence is slow and for thin films, [S] can be assumed to be a constant. To a good approximation, the ratios of the [S] factors for the various elements in a film is also independent of composition. By measuring the ratio of the signal height generated in a spectrum by the various elements of a film, one therefore obtains the elemental concentration ratios of this unknown film. A correction factor must be applied to account for the different (but known) Rutherford scattering cross sections of elements. Alternatively, concentration ratios can also be obtained by comparing the signal heights of a element in two regions of a spectrum corresponding to layers of known and of unknown composition.(6)

All backscattering spectra reported here are presented after such a conversion to concentration profiles (see Fig. 3 to 9). In these profiles, the actual data points are provided at the interfaces only when clear evidence for non-abrupt interface was present. In all other cases, it was presumed that the details in the backscattering spectrum at the interface reflected the finite resolution of the system (detector resolution, energy straggling of the beam) rather than the steepness of concentration variations. The position of these interfaces is therefore indicated by sharp vertical lines only.

B. Seemann-Bohlin X-Ray Diffractometry

A limitation of backscattering spectrometry resides in the fact that the results give atomic concentrations only, without reference to the chemical constitution of the sample. X-ray diffraction analysis can readily identify chemical composition, and thus constitutes an excellent complementary technique to backscattering analysis. Because of the more limited sensitivity of x-ray diffraction, it is advantageous to lengthen the path of x-rays in the thin film by reducing the incident angle. For example, an incident angle of 5° will increase the path length of the beam in the specimen to about 12 times its thickness. In the focusing Seemann-Bohlin arrangement the specimen is placed on the circumference of the diffraction circle. The angle of incidence is fixed and can be made as small as a few degrees. Based on this principle, R. Feder and B. S. Berry have designed and built a 20 inches diameter x-ray diffractometer specifically for thin film studies(7). The diffractometer employs a plyrolytic graphite monochromater crystal to obtain a high intensity monochromatic Cukα radiation, which is incident upon the speciment at an angle of 6.4°.

This diffractometer possesses sufficient sensitivity to resolve the first five diffraction peaks of a copper film of only 150Å thickness using a scan in steps of 0.2° (4θ) and a counting time of 75 sec/step. The broadening exhibited by the diffraction profile is consistent with a particle size of less than 100Å. The diffractometer holds great promise in the investigation of the kinetics of reaction in thin films, because the reaction products can be identified by their x-ray reflections very early in the diffusion cycle, and the rate of change can be measured by changes of their peak intensities.(8) The capability of the diffractometer to determine the lattice parameter very precisely also allows the measurement of stress in a thin film. The measured lattice parameter of a well annealed Ni powder sample was in excellent agreement with the value, a = 3.5283Å (26°C) given in the ASTM file. Using the powder sample as the reference, the stress state of a number of 1000Å Ni films on glass substrates was determined and found to agree with the results obtained by the bending contilever technique(7)

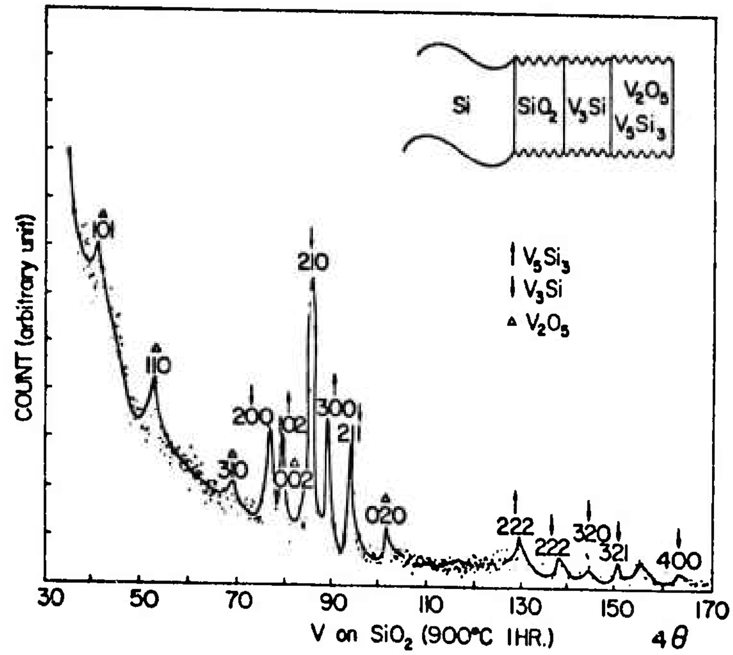

Figure 2. X-ray diffraction pattern of the sample of Fig. 1 after heat treatment. Reflections of V_3Si, V_5Si_3 and V_2O_5 are observed.

We have used the diffractometer to study the reaction products of our transition metal films. The x-ray analyses were performed partly on samples identical with those measured by backscattering, partly on samples identical with those measured by backscattering, partly on samples prepared and annealed under closely similar conditions. For best results, samples of several cm^2 area are required for x-ray measurements, which is typically 10 times the size needed for backscattering analysis. Figure 2 shows a typical x-ray spectrum for a sample of 2000Å of V on an oxidized Si wafer (5000Å of SiO_2) after anneal at 800°C for 30 minutes in vacuum. The spectrum was obtained by scanning the sample at steps of 0.15° (4θ) increment and with a counting time of 30 sec/step. The peaks have been indexed as reflection of VSi_3, V_5Si_3 and V_2O_5.

C. Sample Preparation

For the experiments on Si substrates, commercially polished wafers of either <100> or <111> orientation and of usual n- and p-type doping levels were employed. Orientation and doping have no detectable influence on the results. Immediately before vacuum evaporation of the metal film, the wafers were etched in a solution of 2 HNO_3:1 HF:2 acetic acid and rinsed in deionized water. The SiO_2 substrates were obtained by thermally oxidizing polished Si wafers at 1100°C in a atmosphere of wet oxygen. All metal films were deposited by vacuum evaporation.

III. REACTIONS WITH Si AND SiO_2 SUBSTRATES

A. Titanium

The result of the reaction of Ti with a Si substrate can be seen in Fig. 3. The zero in the depth scale is placed at an arbitrary reference point within the substrate, and positions between this point and the surface are indicated with thicknesses greater than zero. Figure 3 (top) shows 2700Å of Ti as evaporated on a Si substrate. The bottom part of this figure shows this sample after heat treatment at 600°C for 20 min in a vacuum of better than 10^{-5} Torr. The uppermost layer now contains oxygen which was absorbed by the Ti layer during the storage in air and also during annealing. The spread of the points exhibits the poor sensitivity of the backscattering method for elements of lower mass than that of the substrate. Below the Ti on the surface, an intermediate layer has been formed during anneal. The ratio of Ti to Si in that layer can be easily extracted from this graph to be 1:2. The chemical structure has been clearly identified by x-ray analysis as $TiSi_2$. By comparing these two figures, one observes that the Si concentration in the pure substrate. This shows directly that the density of atoms in this compound is higher than that of Si and the total thickness of the system decreases due to the change in densities after compound formation.

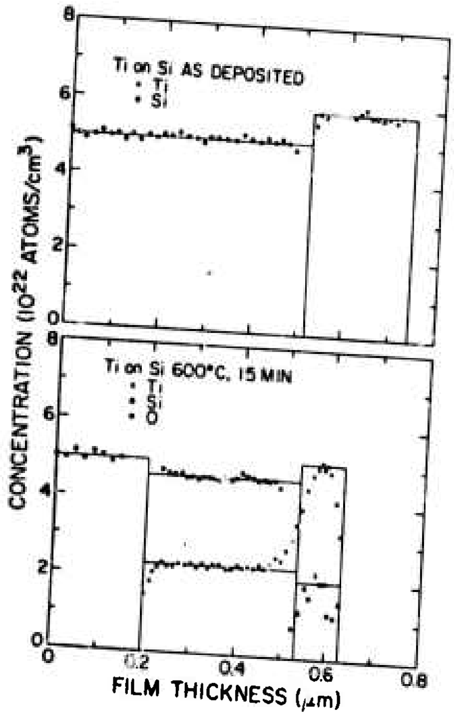

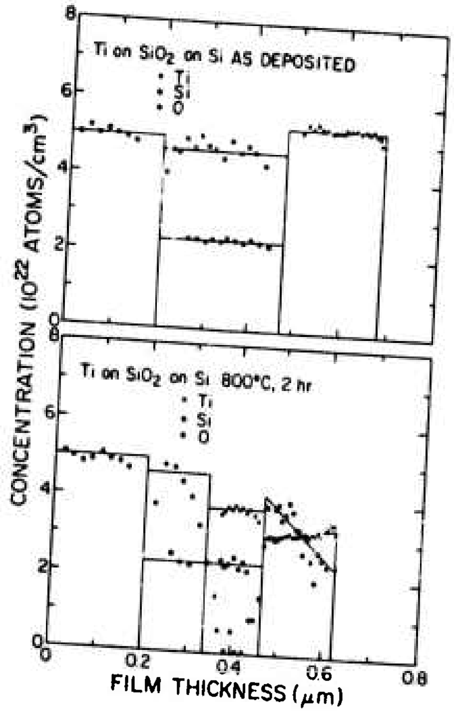

Figure 3. (left) Concentration profile of a Ti film on Si as evaporated (top), and after heat treatment in vacuum at 600°C for 15 minutes (bottom).

Figure 4. (right) Concentration profile of a Ti film as evaporated on an oxidized Si substrate (top), and after heat treatment in vacuum at 800°C for 2 hours (bottom).

The interaction of a vacuum-evaporated Ti film with an amorphous SiO_2 substrate is more complicated, since the metal reacts with a compound. A good example of the complexity of this system is shown in Fig. 4. The top figure gives the concentration profile of a sample after deposition of the metal film, and the figure below shows what happens to that sample after heat treatment at 800°C for 2 hours in vacuum. The surface layer, which was pure Ti before annealing, contains about 50% oxygen after annealing. The layer beneath consist mostly of Si and Ti in a ratio Si:Ti = 0.62. A small amount of oxygen is present also. Its concentration is difficult to evaluate by the backscattering method. Within an accuracy of about 10% the spectrum tells that the amount of oxygen in the surface layer is equal to that originally present in the SiO_2 which reacted with Ti to form a silicide. X-ray analysis could not determine the composition of this Ti-O layer.

B. Vanadium

Far clearer is the interaction of V films with Si and SiO_2. In Fig. 5 the reaction of V with pure Si can be seen. The intermediate layer which grows between the Si substrate and the V film shows two well delineated interfaces in the backscattering spectrum. There is no detectable oxidation of V from the air at room temperature or during annealing in our vacuum system. The backscattering spectrum indicates a ratio of V:Si = 1:2 in the intermediate layer. The x-ray analysis substantiates the result. Only one compound VSi_2 is formed over the whole temperature range from 500°C to 1000°C In addition, the relative intensity ratios of the x-ray diffraction pattern indicate no preferred orientation in the silicide.

At emperatures of 700°C and above V films react with SiO_2, as can be seen in Fig. 6. The various layers observed after the reaction are very well resolved in the backscattering spectra (see Fig. 1). According to this spectrum the surface layer after reaction consists of V and O in the ratio of V:O about 1:1. According to the x-ray data, however, the layer contains V_2O_5 and V_5Si_3. No measurable amount of Si has been found in this layer by Rutherford backscattering analysis. The intermediate layer contains only V and Si. The composition is V:Si = 3:1 from backscattering data and is identified as pure V_3Si by x-ray analysis. The conservation of the total oxygen content in the system is verified within an accuracy better than 10% by comparing the total oxygen amount in layers before and after heat treatment, or by measuring the position of the rear edge of the oxygen signal of the SiO_2 layer. This edge must move if any substance evaporates on or off the surface, or diffuses in or out of the system. This indicates also that no measurable amount of the substrate (Si) diffuses through the SiO_2 layer into the substrate.

C. Niobium (Columbium)

The reaction temperature for Nb films on Si and on SiO_2 prepared at Caltech are higher than 700° and 900°C respectively. Unfortunately, several experimental flaws affect the results. The evaporated layers always contain some oxygen. During heat treatment the oxygen content

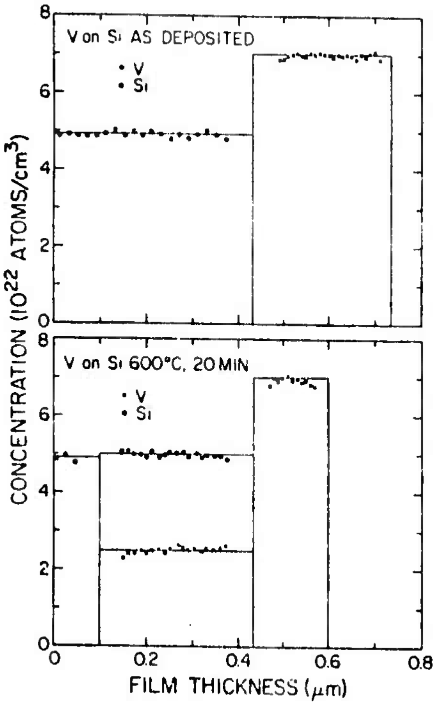

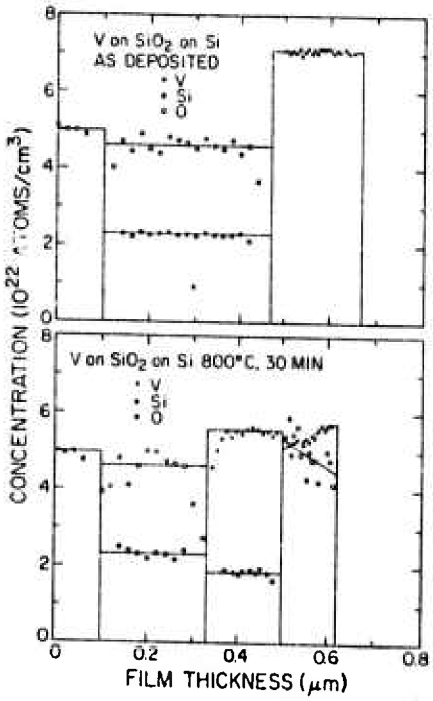

Figure 5. (left) Concentration profile of a V film on Si as evaporated (top), and after heat treatment in vacuum at 600°C for 20 minutes (bottom).

Figure 6. (right) Concentration profile of a V film as evaporated on an oxidized Si substrate (top), and after heat treatment in vacuum at 800°C for 30 minutes (bottom).

increases further. From the best evaporations, we determine for both substrates a ratio for Nb:Si of about 5:3 for the intermediate layers. Since we did not succeed in preparing or maintaining oxygen-free Nb layers, the top layer of Nb has always a noticeable oxygen content.

IV. OXIDATION OF METAL FILMS ON SiO_2

The oxidation products of the metal layers in an oxygen atmosphere have also been studied. The results can be seen in Figs. 7-9.

Ti is known as a very reactive material able to incorporate a remarkable amount of oxygen even at room temperature. We have observed that heat treatment in vacuum tends to homogeneously distribute oxygen throughout the Ti film, indicating that oxygen is very mobile. Heat treatment in dry oxygen atmosphere at 400°C for 2 hours show a total oxygen concentration of about 50% which, however, is not uniform distributed in the layer. But at 600°C, a rapid increase of the oxygen concentration can be seen (Fig. 7, lower part). The layer can be divided into two regions; the top layer shows an oxygen to Ti ratio of about 3:2 and the adjoining region below, which does not reach visibly with the SiO_2 layer at that temperature, has a ratio O:Ti = 1:1.

Vanadium seems to form a compound at relatively low oxidation temperatures. In Fig. 8, the composition of the sample can be seen before (top) and after (bottom) heat treatment at 400°C for 30 minutes in dry oxygen. The transition between the oxide layer and the V metal layer is sharp. The ratio of the oxidized layer is V:O = 2.5, and is identified by x-ray analysis as V_2O_5.

This compound, which is the same as that found by x-ray diffraction in the product of the SiO_2-V reaction, has as low melting point (660°C)[9] To evaluate the effects associated with this melting point, the following experiment has been performed. A V_2O_5 layer, formed by complete oxidation of a V film on SiO_2 at 600°C in dry oxygen, was further heat treated at 700°C in oxygen. The layer melts and forms drops on the surface. The same V_2O_5 layer annealed below 600°C in vacuum shows no visible change. But during an anneal at 640°C in

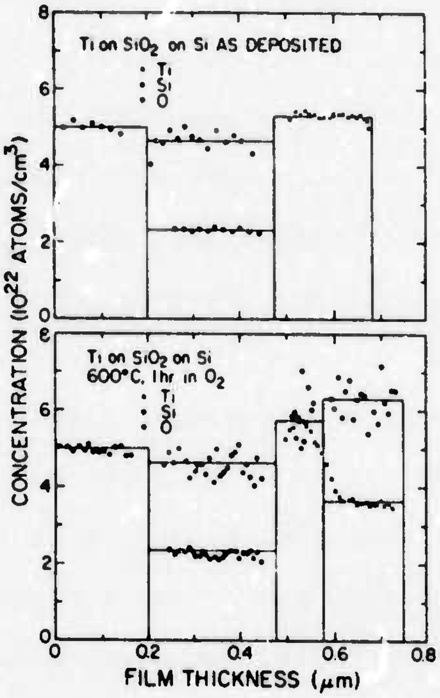

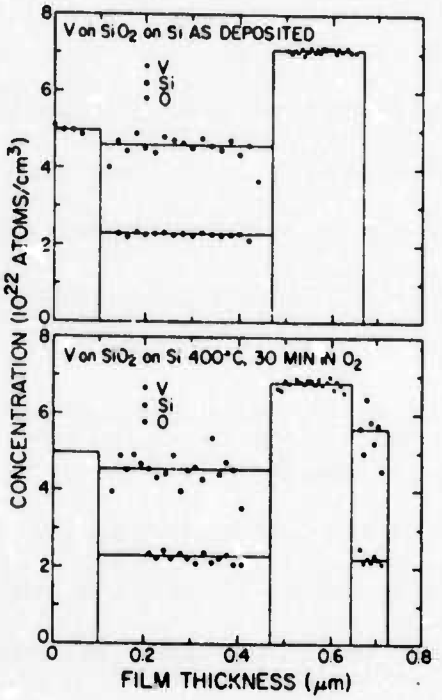

Figure 7. (left) Concentration profile of a Ti film as evaporated on an oxidized Si substrate (top), and after heat treatment in dry oxygen at 600°C for one hour (bottom).

Figure 8. (right) Concentration profile of a V film as evaporated on an oxidized Si substrate (top), and after heat treatment in dry oxygen at 400°C for 30 minutes (bottom).

vacuum for several hours, most of the V_2O_5 layer vaporizes. The behavior of an only partly oxidized V film on SiO_2 as shown in Fig. 8 is different. Up to 600°C in vacuum no change can be seen. But at temperatures higher than 700°C the top layer changes composition. The V:O ratio after annealing for several hours is about 1:1 and below this thick V-O layer is a thin V_3Si layer from the reaction of SiO_2 with the excess V. The V and oxygen content is conserved within the accuracy of the measurement. The same sample has been annealed again in a dry oxygen atmosphere at 400°C and the top layer oxidizes until a ratio of V:O = 2:5 is reached.

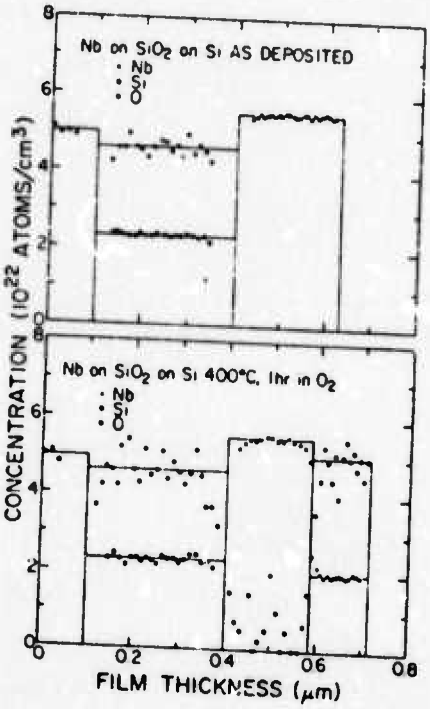

Figure 9. Concentration profile of a Nb film as evaporated on an oxidized Si substrate (top), and after heat treatment in dry oxygen at 400°C for one our (bottom).

After annealing of a Nb film on SiO_2 in oxygen at 400°C, a layer of the composition Nb:O = 2:5 can be found (Fig. 9).

V. DISCUSSION AND CONCLUSION

The binary phase diagrams of these metal-Si systems show that a variety of silicides can exist. For the Si-Ti system four compounds (Ti_3Si, Ti_5Si_3, TiSi, $TiSi_2$), for the Si-V system three compounds (V_3Si, V_5Si_3, VSi_2) and for the Si-Nb system four compounds (Nb_4Si, Nb_3Si, Nb_5Si_3, $NbSi_2$) are reported.(10,11) No prediction can be made what compound will be formed first, if any, by interaction of the elements or by interaction of different compounds at temperatures below the melting point. The phase diagrams of the metal-oxygen systems are even more complicated because of the fact that some of the many possible compounds have large regions of existence.

Table 1. Reaction products of Ti, V and Nb on Si and SiO_2 substrates heat treated in vacuum or in oxygen atmosphere.[2]

		Si	SiO_2		O
		Interface layer (composition)	Interface layer (composition)	Surface layer (composition)	Surface layer (composition)
Ti	Back-Scattering	Ti:Si=0.5	Ti:Si=1.6	Ti:O$\sim$1	Ti:O=0.6
	x-ray	$TiSi_2$	Ti_5Si_3	unidentified	unidentified
	reaction temp.	>500°C		>700°C	600°C
V	back-scattering	V:Si=0.5	V:Si=3	V:O$\sim$1	V:O=0.4
	x-ray	VSi_2	V_3Si	$V_2O_5+V_5Si_3$	V_2O_5
	reaction temp.	>500°C		>700°C	400°C
Nb	back-scattering	Nb:Si$\sim$1.7	Nb:Si$\sim$1.7	Nv:O$\sim$1	Nb:O=0.4
	x-ray	$NbSi_2$*	Nb_3Si*	unidentified	Nb_2O_5
	reaction temp.	>700°C		>900°C	400°C

A summary of the compounds observed in the reaction products between the metal and the Si or SiO_2 substrates, and with oxygen is given in the Table 1. We list the ratio of the elements contained in the films as derived from backscattering analysis. Beneath the backscattering data, the chemical compounds are listed which are identified by glancing angle x-ray measurements. An approximate temperature is also given above which a noticeable reaction rate is observed. Corresponding data of x-ray and of backscattering analyses were all obtained on the identical sample, except where marked by *. The results of the present experiments lead to the following conclusions:

1. Reaction betweena SiO_2 substrate and the metal films requires temperatures which are about 200°C higher than those needed for the reaction of a Si substrate with the same metal film.
2. Silicides formed between metals and Si are generally silicon rich (e.g. VSi_2).
3. Silicides formed between metals and SiO_2 are generally metal-rich (e.g. V_3Si).
4. When metals and SiO_2 react in vacuum, metal silicides and metal oxides are both formed, but in separate layers.
5. Metal oxides produced by reactions with SiO_2 have less oxygen than the metal oxidized formed in an oxidizing ambient.
6. The total amount of Si, oxygen, and metal present in a sample does not change when the reaction takes place in an inert surrounding.
7. No indication of reversibility of the reaction has been observed.

Questions such as how fast the reaction proceeds, what terminates it, and what happen when a given layer is completely consumed are difficult to anewer. Preliminary experiments indicate that some of the complications are due to problems of the cleanness at the interface, and oxygen contamination througout the layers.

ACKNOWLEDGMENTS

This work was supported financially at Caltech by the Air Force Cambridge Research Center (D. E. Davies), and at the IBM Thomas J. Watson Research Center in part by ARPA. Contract No. FI9628-73-C-006 administered by the Air Force Cambridge Research Laboratories. We also thank the Kellogg Radiation Laboratory at Caltech for the use of the 3 MeV accelerator, and in particular Dr. C. A. Barnes for his continuous assistance in the backscattering measurements.

REFERENCES

1. R. W. Bower, Appl. Phys. Lett. 23, 99 (1973).
2. K. N. Tu, J. F. Ziegler and C. J. Kircher, Appl. Phys. Letters 23, 493 (1973)
3. B. Schwartz (Ed.), "Ohmic Contacts to Semiconductors", The Electrochemical Society, (New York, 1969).
4. L. J. Schwartz, Ph.D. Thesis, The City University of New York, 1970.
5. H. Kräutle, M-A. Nicolet and J. W. Mayer, Phys. Stat. Sol. (a) (submitted).
6. W. K. Chu, J. W. Mayer, M-A. Nicolet, T. M. Buck, G. Amsel and F. Eisen, Thin Solid Films 17, 1 (1973).
7. R. Feder and B. S. Berry, J. Appl. Cryst. 3, 372 (1970).
8. K. N. Tu and B. S. Berry, J. Appl. Phys. 43, 3283 (1970).
9. Gmelins Handbuch der anorganischen Chemie, Vol. 41, 48 and 49, (Verlag Chemie GMBH, Weinheim 1951).

10. M. Hansen, Constitution of Binary Alloys, (McGraw-Hill, 1958).

11. F. A. Shunk, Constitution of Binary Alloys, second supplement (McGraw-Hill, 1969).